Electrical Power and Energy Systems 172 (2025) 111093

Contents lists available at ScienceDirect

International Journal of Electrical Power and Energy Systems

journal homepage: www.elsevier.com/locate/ijepes

Two-stage robust optimization strategy for VPP participation in the energy and reserve markets considering intertemporal carbon trading

Hadi Nemati *, Álvaro Ortega, Pedro Sánchez-Martín

Institute for Research in Technology, Comillas Pontifical University, Spain

ARTICLE INFO

Keywords:
Virtual power plant
Carbon trading market
Energy market
Secondary reserve market
Robust optimization

ABSTRACT

This paper proposes a coordinated strategy for Virtual Power Plants (VPPs), including both renewable and conventional units, to participate in the Day-Ahead Market (DAM) and Secondary Reserve Market (SRM), while incorporating intertemporal Carbon Trading Market (CTM) constraints. The model enables the VPP to leverage differences in CTM prices across multiple sample days by strategically selling excess carbon credits or purchasing required credits on sample days with more favorable prices. A two-stage robust optimization framework is developed to account for multiple uncertainties in market prices, renewable energy production, and demand consumption. The proposed scheduling strategy encourages the VPP to prioritize low-emission resources and limit the use of polluting units, contributing to both profitability and emission reduction. To evaluate the effectiveness of the proposed approach, simulations are conducted for a 220 MW VPP supplying 80 MW of internal demand under various uncertainty-handling strategies and carbon credit allowance levels. The findings show that the proposed model enables more flexible carbon trading, with CTM-related profitability increasing by 29.0–55.3%, and carbon emissions reduction improvement up to 8.9% compared to daily carbon trading.

1. Introduction

1.1. Motivation

The Virtual Power Plant (VPP) is a coordinated system of Renewable Energy Sources (RES), conventional units, and Flexible Demands (FDs), integrated through advanced control and communication technologies. By aggregating these heterogeneous assets, a VPP can provide ancillary services, manage local imbalances, and enhance system reliability, while participating in wholesale electricity markets with a unified bidding strategy. This aggregation not only facilitates the economic integration of variable RES but also enables smaller units to access markets that would otherwise be unavailable to them individually [1].

On another front, the European Union Emissions Trading System (EU ETS) has played a central role in driving decarbonization across major carbon-intensive sectors since its inception in 2005. With a cumulative reduction of 47% in greenhouse gas emissions by 2023 and an increased ambition for a 62% cut by 2030, the EU ETS has proven effective in transitioning the power sector toward cleaner generation. The tightening cap and rising carbon prices – coupled with the expansion of ETS coverage – highlight the growing relevance of the Carbon Trading Market (CTM) [2]. As carbon regulations become increasingly stringent, the VPPs – particularly those integrating thermal units – must revise their operational strategies to account for potential emissions from each unit, carbon allowance volatility, and broader sustainability considerations. This highlights the need to embed environmental constraints directly into their modeling and decision-making frameworks. Their integrated control over both renewable and conventional generation allows them to adapt dispatch strategies to minimize emissions, promoting environmentally sustainable outcomes. VPPs can also capitalize on their flexibility not only to optimize participation in electricity markets but also to strategically engage in carbon trading. Such dual participation enhances revenue potential while supporting systemic emissions reduction, aligning economic incentives with environmental goals [3].

In European electricity markets, the Day-Ahead Market (DAM) enables producers and consumers to submit hourly bids for the next day, with market clearing typically occurring 12 h before delivery [4]. Alongside, the Secondary Reserve Market (SRM) ensures grid stability by procuring fast-response reserves, where certified units provide automatic frequency restoration services under strict response and duration requirements [5]. Leveraging their operational flexibility, VPPs can engage in both DAM and SRM to boost profitability. Meanwhile, the CTM – as part of the EU ETS – regulates emissions through a cap-and-trade mechanism. Allowances are distributed based on historical

* Corresponding author.
E-mail address: hnemati@comillas.edu (H. Nemati).

https://doi.org/10.1016/j.ijepes.2025.111093
Received 24 May 2025; Received in revised form 8 August 2025; Accepted 4 September 2025
Available online 17 September 2025
0142-0615/© 2025 The Author(s). Published by Elsevier Ltd. This is an open access article under the CC BY-NC-ND license (http://creativecommons.org/licenses/by-nc-nd/4.0/).

The general notation used in this paper is outlined below. A detailed nomenclature, including definitions of all variables and parameters, is provided in Appendix A.

General Nomenclature

Notation Concepts

- An uncertain parameter with a tilde symbol denotes the median value in the forecast distribution ($\tilde{A}$);
- an uncertain parameter with a tilde and hat/inverse hat symbol denotes the upper/lower bound in the forecast distribution ($\hat{\tilde{A}}/\check{\tilde{A}}$);
- the hat/inverse hat symbol on uncertain parameters signifies the positive/negative permitted deviation from the forecast's value ($\hat{A}$, $\check{A}$);
- parameters with an upper/lower bar represent their upper/lower bounds ($\bar{A}$, $\underline{A}$);
- upward/downward arrows indicate up/down direction of regulation in variables and parameters ($a^{\uparrow}$, $A^{\uparrow}/a^{\downarrow}$, $A^{\downarrow}$);
- positive/negative symbol on variables and parameters indicates the charging/discharging state of storage (a^{+}, A^{+}/a^{-}, A^{-}).

Abbreviations

CCO	Chance-Constrained Optimization	MILP	Mixed Integer Linear Programming
C&CG	Column & Constraint Generation	PV	Photovoltaic
CSP	Concentrated Solar Power Plant	RES	Renewable Energy Sources
CTM	Carbon Trading Market	RO	Robust Optimization
CVaR	Conditional Value-at-Risk	SF	Solar Field
DAM	Day-Ahead Market	SO	Stochastic Optimization
ES	Electrical Storage	SRM	Secondary Reserve Market
ETS	Emissions Trading System	TS	Thermal Storage
EV	Electric Vehicle	TPP	Thermal Power Plant
FD	Flexible Demand	VPP	Virtual Power Plant
IGDT	Information Gap Decision Theory	WF	Wind Farm

Indexes and Sets

$t \in \mathcal{T}$	Set of time periods in each sample day
$t \in \mathcal{T}^{Day}$	Set of sample days
$u \in \mathcal{U}$	Set of VPP units

Parameters

C_u	Operation costs of unit u	[€/MWh]
E_u	Electrical energy of unit u	[MWh]
P_u	Electrical or thermal power forecast or capacity of unit u	[MW]
R_u^{SR}	Secondary reserve ramp rate of unit u	[MW/min]
α_u	Emission factor of unit u	[tons CO_2/MW]
Γ	Uncertainty budget	[–]
Δt	Duration of periods	[hour]
η_u	Electrical or thermal power efficiency of unit u	[%]
ι_u	Emission quotas for unit u	[tons CO_2/MW]
κ	Percentage of reserve traded in the SRM relative to the power capacity of VPP	[%]
λ_t	Market price during period or sample day t	[€/MW or €/MWh or €/tons CO_2]

Variables

$e_{u,t}$	Electrical energy of unit u during period t	[MWh]
n_t^{CT}	Carbon credits traded by VPP in the CTM during sample day t	[tons CO_2]
$n_{u,t}$	Carbon credits required by unit u during period or sample day t	[tons CO_2]
p_t^{DA}	Electrical power traded by VPP in the DAM during period t	[MW]
$p_{u,t}$	Electrical or thermal power of unit u during period t	[MW]
r_t^{SR}	Reserve traded by VPP in the SRM during period t	[MW]
$r_{u,t}$	Reserve provided by unit u during period t	[MW]
z_t	Positive auxiliary variable of uncertain parameters during period t	[MW or MWh or tons CO_2]
w_t	Positive auxiliary variable of uncertain parameters during period t	[–]
δ	Dual variable to model the uncertain parameters	[€ or MW]
ψ_t	Dual variable to model uncertain parameters during period t	[€ or MW]
$u_{u,t}$	Binary variable for on/off status of unit u during period t	[–]
$v_{u,t}^{SU/SD}$	Binary variable for start-up/shut-down status of unit u at period t	[–]
$\chi_{u,t}$	Binary variable to model unit u worst case occurrence during period t	[–]

activity and performance benchmarks, with participants required to cover annual emissions by holding or trading sufficient credits [6]. VPPs incorporating fossil-fueled units or industrial demand can participate in carbon trading, adding both environmental value and an additional revenue source to their operations.

VPPs operate within a highly uncertain environment influenced by market price volatility, renewable generation variability, and load fluctuations [7]. Although the aggregation of diverse units inherently smooths some of this variability, effective uncertainty modeling remains crucial. To ensure effective market participation, optimization tools must be both computationally efficient and adaptable to the operator's risk preferences [8]. Therefore, a comprehensive strategy should account not only for electricity markets and emissions-related considerations but also for unit-specific technical characteristics and the impact of uncertainties. These elements are essential to fully exploit the capabilities of VPPs.

1.2. Literature review

The operation and bidding of VPPs in electricity energy market have been extensively explored in the literature [9–12]. An industrial VPP integrating RES, Electrical Storage (ES), and process-linked storage is proposed in [9], where scenario-based Stochastic Optimization (SO) models best- and worst-case uncertainties using Conditional Value-at-Risk (CVaR). In [10], scenario-based SO is used to capture uncertainties in price, RES output, and energy demands, incorporating both RES and conventional sources. In contrast, [11] adopts a deterministic bi-level framework for multi-energy VPP bidding, while [12] introduces a rolling horizon optimization approach for VPP operations in DAM and intra-day market, focusing on RES intermittency and market-aggregator dynamics.

Further studies explore VPP participation in ancillary markets beyond energy trading to enhance profitability. In [13], a two-stage Robust Optimization (RO) model is developed and solved using the Column & Constraint Generation (C&CG) algorithm for a multi-energy VPP participating in the peak regulation market, accounting for uncertainties in Photovoltaic (PV) generation and demand fluctuations. A bi-level SO framework in [14] enables distributed VPPs to trade both in wholesale electricity markets and peer-to-peer setups, accounting for RES and demand-side uncertainties. A robust single-level Mixed Integer Linear Programming (MILP) model is proposed in [15] for simultaneous energy and reserve markets, targeting worst-case profit under uncertainties in prices, RES output, and demand. Additionally, [8] employs average regret as a risk measure for VPP decision-making under uncertainty. The paper [16] introduces a hybrid RO-SO approach for optimal scheduling in integrated electricity and thermal markets, addressing uncertainties in renewable generation and consumption patterns. The above studies focus solely on the economic aspects of the VPP problem and overlook environmental concerns. However, to support climate goals, VPP models must integrate financial viability with environmental considerations such as carbon emission reduction and low-carbon scheduling.

The joint consideration of environmental factors and economic objectives in VPP operation – particularly through coordinated participation in electricity markets and the CTM – has been explored in the literature. The work in [17] proposes a deterministic economic dispatch model for a VPP that integrates both green certificate trading and carbon trading to support low-carbon and economic goals. In [18], a deterministic bidding strategy is formulated for VPP participation in energy, reserve, and CTM, with carbon credits traded at fixed prices. The study in [19] develops an optimal scheduling model for VPP operations under green certificate trading and carbon trading, using a Particle Swarm Optimization (PSO) algorithm to optimize environmental and economic outcomes. In [20], a cooperative game-based strategy is introduced for VPP participation in joint electricity and CTM, with the deterministic bidding problem solved via the Whale Optimization Algorithm (WOA). The study in [21] addresses the optimal scheduling of a VPP comprising Wind Farm (WF), solar PV, gas turbine, and ES, incorporating both carbon trading and green certificate trading. The problem is solved using the PSO algorithm, and the analysis focuses on carbon emissions and RES utilization over four sample days. However, a fixed CTM price is assumed, and interactions between the sample days are not considered. The paper [22] proposes a multi-objective bidding strategy for a multi-energy VPP in energy, frequency regulation markets, and the CTM, balancing economic performance with consumer satisfaction, although uncertainties are not considered. The above studies adopt a deterministic approach and overlook the impact of key uncertainties, such as market prices, RES production, and demand consumption, on VPP operations. However, these uncertainties can significantly affect both profitability and carbon emissions of the units and should be explicitly considered for more realistic and robust decision-making.

Some studies address the uncertainties in RES generation and demand consumption when optimizing the joint participation of VPP in electricity markets and CTM. In [23], a multi-objective operation model for a multi-energy VPP including ES and Thermal Storage (TS) is developed to jointly maximize profit and minimize carbon emissions, incorporating uncertainties in electricity prices, PV and WF output, and demand consumption via a scenario-based approach. The work in [24] proposes a dispatch strategy aimed at near-zero carbon emissions for a rural VPP composed of gas turbine, gas storage, biomass, rooftop PVs, and distributed wind units. Uncertainties in RES and load are managed using Information Gap Decision Theory (IGDT), and a cooperative game framework addresses economic, risk, and environmental objectives. This approach is extended in [25], which integrates green certificate trading through a data-driven two-stage RO model. In [26], a data-driven distributed RO framework is introduced for VPP bidding in energy markets under a ladder-type carbon trading scheme, using scenario-based uncertainty modeling and clustering. The study in [27] considers a multi-microgrid VPP to enhance economic and low-carbon performance, employing a three-stage scheduling model across DAM and real-time market, with carbon emissions allocated daily among VPP units. A two-stage RO model is proposed in [28] for optimal dispatch under RES and demand uncertainty, integrating a carbon trading mechanism to balance cost and emissions. The paper [29] develops a VPP model including carbon capture systems operating in electricity, carbon, and natural gas markets. Market uncertainties are addressed using CVaR, and the multi-objective model is solved with a collaborative evolutionary algorithm. In [30], a bi-level model is developed to determine the pricing strategy for an Electric Vehicle (EV)-based VPP participating in energy markets, ancillary service, and the CTM. Renewable energy uncertainty is addressed using a SO approach with CVaR, and carbon quotas are allocated to both TPPs and EVs, where EV emissions are estimated based on equivalent fuel vehicle emissions. The study in [31] introduces an incentive-based demand response mechanism to reduce carbon emissions from a VPP operating in the energy and reserve DAM and the CTM. Uncertainties in RES generation are handled using a Chance-Constrained Optimization (CCO) method. In [3], a joint market participation strategy is proposed for a VPP in the DAM, real-time market, reserve market, and CTM, where a RO framework accounts for uncertainties in RES generation, load demand, and market prices. These studies typically model VPP operations based on a single sample day, during which the CTM price is assumed to be fixed due to its limited daily variability. However, by restricting the analysis to such a time horizon, they overlook intertemporal carbon trading constraints and their potential impact on trading strategies, unit scheduling, profitability, and emissions.

Although considerable research has addressed the participation of VPPs in electricity markets and the CTM, many existing studies rely on simplified models that assume a single carbon price and a single sample day. Such approaches constrain the VPP to buy or sell carbon credits based solely on a static snapshot, overlooking the intertemporal nature of carbon trading. Since carbon quotas are typically assigned on an annual basis and units must present sufficient credits yearly rather than daily, this necessitates an annual perspective in credit management. Furthermore, VPP operational schedules vary throughout the year due to fluctuations in RES availability and load demand. As a result, it is essential to account for diverse scheduling patterns, temporal flexibility in trading decisions, and uncertainty in CTM prices. To address these limitations, this paper proposes a comprehensive joint market participation model for VPP operations across energy and reserve electricity markets while explicitly considering the intertemporal constraints of carbon trading.

A four-sample-day framework that captures seasonal variations by considering interactions among sample days is employed. The model enables the VPP to optimize its carbon trading strategy by selecting the most economically advantageous sample days for trading, rather than being constrained to a fixed trading period. To handle inherent

Table 1
Summary of key differences between the proposed approach and related literature.

Ref.	Components				Market		Uncertainty				CTM model	Intertemporal CTM constraints	Method & solution
	Renew-able	Conven-tional	Storage	Flexible load	Energy & reserve	CTM	Electricity	CTM	Renew-able	Load			
[9]	WF	✓	✓	×	×	×	✓	×	✓	×	×	×	SO, CVaR
[10]	PV/WF	✓	✓	×	×	×	✓	×	✓	✓	×	×	SO, MILP
[11]	PV/WF	✓	×	×	×	×	×	×	×	×	×	×	Nonlinear
[12]	PV/WF	✓	✓	✓	×	×	×	×	✓	✓	×	×	Nonlinear
[13]	PV	✓	✓	×	×	×	×	×	✓	✓	×	×	Two-stage RO, C&CG
[14]	PV/WF	×	✓	✓	✓	×	×	×	✓	✓	×	×	Two-stage SO, MILP
[15]	PV/WF	×	×	✓	✓	×	✓	×	✓	✓	×	×	RO, MILP
[8]	PV/WF	×	✓	✓	✓	×	✓	×	✓	✓	×	×	RO, MILP
[16]	PV/WF	×	✓	✓	×	×	×	×	✓	✓	×	×	Two-stage RO-SO, C&CG
[17]	PV/WF	✓	✓	×	×	✓	×	×	×	×	1 sample day	×	MILP
[18]	PV/WF	✓	✓	✓	✓	✓	×	×	×	×	1 sample day	×	Non-linear
[19]	PV/WF	✓	×	✓	×	✓	×	×	×	×	1 sample day	×	PSO
[20]	PV/WF	✓	✓	✓	×	✓	×	×	×	×	1 sample day	×	Non-linear, WOA
[21]	PV/WF	✓	✓	×	×	✓	×	×	×	×	4 sample days w/o interactions	×	Non-linear, PSO
[22]	WF	✓	✓	✓	✓	✓	×	×	×	×	1 sample day	×	Non-linear, Fuzzy
[23]	PV/WF	✓	✓	✓	✓	✓	✓	×	✓	✓	×	×	SO, MILP
[24]	PV/WF	✓	✓	✓	×	✓	×	×	✓	✓	1 sample day	×	MILP, IGDT
[25]	PV/WF/ Hydro	✓	✓	✓	×	✓	×	×	✓	✓	1 sample day	×	Data-driven, MILP Two-stage RO, C&CG
[26]	PV/WF	✓	✓	✓	×	✓	×	×	✓	✓	1 sample day	×	Data-driven, SO-RO
[27]	PV/WF	✓	✓	✓	×	✓	×	×	✓	✓	1 sample day	×	SO, MILP
[28]	PV/WF	✓	✓	✓	×	✓	×	×	✓	✓	1 sample day	×	Two-stage RO, C&CG
[29]	PV/WF	✓	✓	✓	×	✓	✓	×	×	×	1 sample day	×	CVaR, Non-linear
[30]	PV/WF	✓	✓	✓	✓	✓	×	×	✓	×	1 sample day	×	SO, CVaR, MILP
[31]	WF	✓	✓	✓	✓	✓	×	×	✓	×	1 sample day	×	CCO, MILP
[3]	WF	✓	✓	✓	✓	✓	✓	×	✓	✓	1 sample day	×	RO, MILP
This paper	PV/WF/ CSP	✓	✓	✓	✓	✓	✓	✓	✓	✓	4 sample days with interactions	✓	Two-stage RO, MILP

uncertainties, a two-stage RO formulation is developed, incorporating stochasticity in DAM and SRM electricity prices, CTM prices, RES generation, Concentrated Solar Power Plant (CSP) thermal energy generation, and FD consumption. The proposed model uses a set of tunable parameters – referred to as uncertainty budgets – that allow the VPP operator to calibrate the degree of protection applied to each uncertain parameter. This feature ensures that the model can adapt its level of conservatism based on the operational impact of each source of uncertainty, leading to more informed and flexible decision-making. In comparison to existing studies, this paper introduces a more comprehensive framework for VPP participation in energy and reserve markets by incorporating a broader range of uncertainties and enabling greater flexibility in carbon trading decisions. To support this contribution, Table 1 presents a comparative analysis of the key features of the reviewed literature alongside those of the proposed model.

1.3. Paper contributions

Addressing the shortcomings in the literature, this work introduces the following primary contributions:

- *To model intertemporal carbon credit trading in the VPP problem:* Existing literature typically models carbon credit trading on a daily basis with a fixed price, which limits trading decisions to the same day the emissions are generated. Some studies consider multiple sample days to analyze the carbon emissions and trading performance of a VPP, but they do not account for the long-term effects of carbon trading strategies or the intertemporal interactions between different sample days. However, in practice, carbon credits are often allocated on an annual basis, and the VPP can leverage the intertemporal effects to enhance its overall profitability. To better reflect this, the proposed model incorporates carbon credit trading across four sample days with varying CTM prices. This approach allows the VPP to plan and trade credits based on a long-term emission strategy. The intertemporal modeling enables the VPP to offset emissions from high-pollution sample days by purchasing credits on sample days with lower carbon costs or by selling excess credits on sample days with higher CTM prices.
- *To develop a two-stage flexible RO formulation that considers multiple uncertainties within a multi-market VPP framework:* Although two-stage RO models exist in the literature, a comprehensive framework that considers both short-term and long-term uncertainties in the VPP problem – covering energy and reserve markets as well as the CTM – has not yet been proposed. Accordingly, this paper addresses several sources of uncertainty, including DAM prices, SRM prices, CTM prices, RES production, and industrial FD consumption, by proposing a two-stage RO model. In the first stage, the VPP operator determines the unit commitments and trading decisions for energy, reserve, and carbon credits across different

markets. In the second stage, the aforementioned uncertainties impact the objective function. The model allows the VPP operator to flexibly adjust its level of conservatism in response to each uncertainty through the use of uncertainty budget parameters. Accordingly, a wide range of decision approaches (from optimistic to pessimistic) are examined across multiple sample days, and their effects on the VPP's energy and reserve trading strategy, carbon credit trading, carbon emissions, and optimal scheduling decisions are analyzed.

- *To design an emissions-aware scheduling model for VPP units:* In traditional approaches in the literature, the VPP considers only the carbon price of each specific day and may choose to operate in a high-emission mode when credit prices are low, thereby missing the opportunity to optimize over a longer horizon. In contrast, the approach proposed in this paper promotes a more environmentally friendly operation of VPP units compared to single-day or multi-day models that do not account for intertemporal interactions. Accordingly, this paper presents a scheduling model for various units of the VPP, including WF, solar PV, CSP, TS, ES, and FD, across different sample days. The proposed framework incentivizes emission reductions by prioritizing the dispatch of RES units and preserving carbon credits for more profitable trading opportunities—achieved by selecting favorable sample days for carbon credit trading. As a result, the VPP is encouraged to limit the operation of polluting units, such as the Thermal Power Plant (TPP) and industrial demand, not only to enhance profitability but also to support the carbon neutrality of the power grid.

2. Problem description

The primary objective of a VPP is to facilitate the integration of RES into electricity markets while operating dispatchable fossil-based units efficiently to support carbon neutrality goals. To achieve this, the VPP must actively participate in multiple markets, including the DAM, SRM, and CTM. It must also manage diverse uncertainties, such as price volatility, renewable output variability, and demand fluctuations. The central task is to determine optimal scheduling and bidding strategies that maximize profit, maintain emissions within regulated limits, and ensure the reliable operation of its stochastic units. Fig. 1 presents the overall architecture, illustrating the VPP components, their interactions, and the proposed optimization framework.

The VPP may integrate solar PV plants, WFs, CSPs with TS, ESs, TPPs along with FDs. The operator collects forecast data and technical constraints from these units and communicates their schedules based on market outcomes. As all units are connected to grid for energy and reserve trading, the VPP can participate in both the DAM and SRM. Since these short-term markets operate on a daily basis, the VPP submits independent bids for each sample day, capturing different production and consumption patterns. Market clearing in the DAM is managed by the market operator. The SRM, on the other hand, is coordinated by the transmission system operator, which allocates reserves through secure economic dispatch and accepts offers to maintain real-time system balance [5,32]. Given its small size relative to the overall market, the VPP is modeled as a price taker, and price forecasts are derived from historical data.

Under the EU ETS, carbon allowances are allocated annually to emitting units based on predefined criteria. Each unit must surrender sufficient credits to match its verified yearly emissions. The VPP can participate in the CTM by trading carbon credit allowances, with each credit corresponding to the offset of 1 ton of CO_2 emissions from polluting units [6]. While carbon credit trading provides flexibility for VPPs, relying on short-term trading strategies – such as daily or opportunistic purchases – can be both environmentally inefficient and economically suboptimal. In periods of low carbon prices, thermal units may be dispatched at low cost but with high emissions, undermining sustainability goals. Conversely, when carbon prices rise, emission reductions may occur but at a significantly higher cost. Such short-term approaches fail to consistently support either cost efficiency or environmental responsibility.

In contrast, an annual approach, as adopted in this study, provides a more consistent alignment with emissions constraints and long-term decarbonization targets. Incorporating carbon trading into strategic scheduling decisions enables VPPs to optimize their operations while maintaining environmental responsibility. Moreover, as EU ETS regulations evolve to reduce the total volume of allowances and increase the carbon price floor, VPPs must increasingly prioritize low-emission units and minimize dependence on carbon-intensive generation. From a policy perspective, long-term models that incorporate emissions constraints and sustainability metrics are better aligned with EU climate goals [6]. Therefore, a long-term approach that integrates both operational costs and environmental aspects is essential to ensure that VPPs contribute not only to market efficiency but also to systemic emissions reduction.

Given this context, although the CTM is traded daily – often at a fixed price – it is more effective for VPP operators to schedule fossil-based units on an annual basis. This is also due to seasonal variations in RES output and demand, which lead to different levels of pollution. Additionally, given long-term carbon price volatility, acquiring or selling credits strictly on the sample day when emissions occur is suboptimal. Instead, VPP operators may procure credits during low-price periods (sample days) and emit during high-price periods. To prevent market manipulation, the model in this paper restricts carbon trading to the net difference between total emissions and the allocated annual allowance, disallowing the purchase or sale of credits beyond this margin. This ensures that credits cannot be repeatedly bought and sold across seasons to exploit price fluctuations.

The VPP operator manages energy scheduling for all units by solving the proposed optimization framework. This is based on each unit's technical specifications, forecasted RES generation, price forecasts, and market conditions. The objective is to maximize total profit from energy and reserve trading in the DAM and SRM, as well as carbon credit transactions in the CTM, while accounting for operational costs. The model incorporates both deterministic and uncertainty-driven constraints. Deterministic constraints include supply–demand balance, carbon emission and credit trading limits, and operational constraints of units with dispatchable outputs such as TPPs and ESs. They also include the deterministic operation constraints of units with stochastic behavior (e.g., PV, WF, CSP, and FDs). In contrast, uncertainty-related constraints capture the variability in power output from RES and demand-side units, as well as uncertain market prices in the DAM, SRM, and CTM.

To address the adverse effects of uncertainty on the VPP operator's profit, a two-stage RO framework is employed [13]. The first stage determines optimal scheduling and bidding decisions to maximize expected profit, while the second stage evaluates the worst-case realizations of uncertain parameters within a specified uncertainty set. This set is controlled by an *uncertainty budget*, a tunable parameter that reflects the operator's risk *appetite* [8]. For short-term uncertainties – such as RES output, demand, and DAM/SRM prices – the budget defines the number of hours per sample day that may experience worst-case deviations. In contrast, for long-term uncertainties like CTM prices, it indicates the number of sample days subject to extreme values. By adjusting these budgets, the operator can balance robustness and performance. Upon solving the model, the VPP operator obtains the internal dispatch plan, market bids for energy and reserves, and carbon credit trading quantities for submission to relevant units and market platforms. The interested reader is referred to [15] for a comprehensive discussion on the impact of the uncertainty budget.

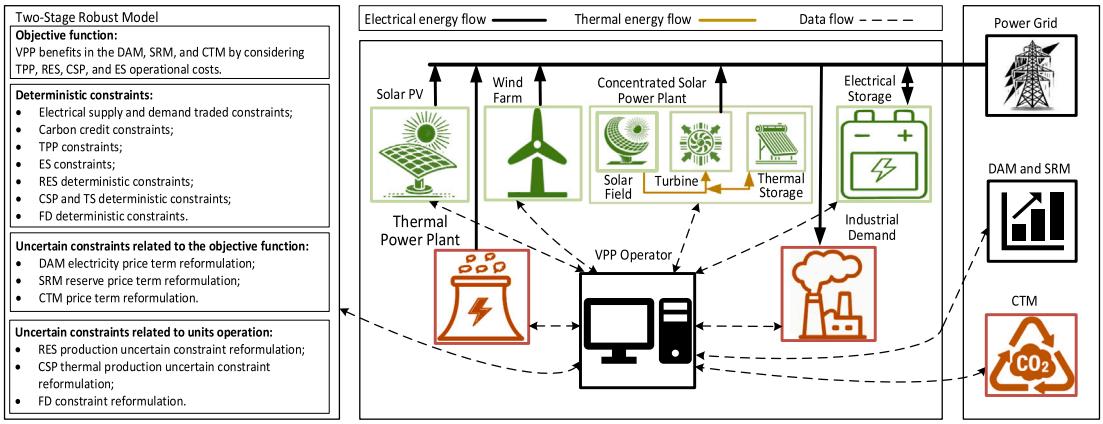

Fig. 1. The scheme of considered VPP for participation in DAM, SRM, and CTM.

3. Two-stage robust optimization framework

The optimization framework must account for the technical characteristics of the units, market structures, environmental factors, and various sources of uncertainty. The two-stage RO approach effectively addresses these aspects by dividing the decision-making process into two stages. The first stage defines the VPP's initial market bids and operational plans. The second stage adapts to the worst-case realization of uncertain parameters, ensuring feasibility and robustness under adverse conditions [13]. To support the mathematical formulation presented in this section, Fig. 2 illustrates the interactions among VPP components, various markets, decision stages, and sources of uncertainty in the proposed two-stage RO framework. Accordingly, this section develops a two-stage RO optimization framework to model the VPP's decision-making process under uncertainty, aiming to maximize profitability while complying with operational, environmental, and market constraints. The deterministic formulation, which assumes fixed values for uncertain parameters, is presented in Section 3.1, whereas the two-stage RO approach, which considers uncertainties from the source and load sides as well as market prices, is elaborated in Section 3.2.

3.1. Deterministic problem

The deterministic formulation models the operation and bidding of the VPP in the electrical energy and reserve markets, as well as in the CTM by assuming fixed values for uncertain parameters. This section presents the deterministic objective function along with the constraints related to the VPP's technical units, market participation, and carbon emission considerations in the optimization problem. This provides a clear foundation for understanding the problem structure before incorporating uncertainty, which is addressed in the RO model formulation in Section 3.2.

3.1.1. Objective function

The deterministic objective function, presented in (1), seeks to maximize the VPP's profits in the DAM, SRM, and CTM, while incorporating the operational costs of its units [33]. The first term in (1) captures the expected revenues from the VPP's bids in the DAM. The second term computes the expected revenue from both upward and downward SRM. The third term reflects revenues obtained from CTM. The fourth and fifth terms denote the operational costs of RES and CSPs, respectively. The seventh term calculates the operational costs of TPPs, including their start-up and shut-down costs. Finally, the last term represents the degradation cost of ESs.

$$\max_{\Xi^{DA+SR+CT}} \sum_{t\in\mathcal{T}} \lambda_t^{DA} p_t^{DA} \Delta t + \sum_{t\in\mathcal{T}} \left[\lambda_t^{SR,\uparrow} r_t^{SR,\uparrow} + \lambda_t^{SR,\downarrow} r_t^{SR,\downarrow}\right] + \sum_{t\in\mathcal{T}^{Day}} \lambda_t^{CT} n_t^{CT} - \sum_{t\in\mathcal{T}}\sum_{r\in\mathcal{R}} C_r p_{r,t} \Delta t - \sum_{t\in\mathcal{T}}\sum_{\theta\in\Theta} C_\theta p_{\theta,t} \Delta t - \sum_{t\in\mathcal{T}}\sum_{c\in\mathcal{C}} \left[C_c p_{c,t} \Delta t + C_c^{SU} v_{c,t}^{SU} + C_c^{SD} v_{c,t}^{SD}\right] - \sum_{t\in\mathcal{T}}\sum_{s\in\mathcal{S}} M_s \frac{C_s}{\bar{E}_s} p_{s,t} \Delta t \quad (1)$$

3.1.2. Electrical supply & demand traded constraints

The equality constraint that ensures the supply–demand balance of electrical energy and reserve for VPP units is specified in (2a).[1] This constraint considers all potential reserve activation scenarios in real-time, such as upward reserve activation, downward reserve activation, and no reserve activation. To represent these scenarios, vectors $\boldsymbol{r}_t^{SR} = \{r_t^{SR,\uparrow}, -r_t^{SR,\downarrow}, 0\}$; $\boldsymbol{r}_{r,t} = \{r_{r,t}^{\uparrow}, -r_{r,t}^{\downarrow}, 0\}$; $\boldsymbol{r}_{\theta,t} = \{r_{\theta,t}^{\uparrow}, -r_{\theta,t}^{\downarrow}, 0\}$; $\boldsymbol{r}_{c,t} = \{r_{c,t}^{\uparrow}, -r_{c,t}^{\downarrow}, 0\}$; $\boldsymbol{r}_{s,t} = \{r_{s,t}^{\uparrow}, -r_{s,t}^{\downarrow}, 0\}$; and $\boldsymbol{r}_{d,t} = \{r_{d,t}^{\uparrow}, -r_{d,t}^{\downarrow}, 0\}$ are defined for the VPP, RES, CSP, TPP, ES, and FD. As a result, (2a) comprises a set of three equations. The upper and lower limits for the total electrical energy and reserve traded by the VPP are regulated by Eqs. (2b) and (2c), respectively. The traded upward and downward reserves of the VPP are constrained by a fraction of its maximum electrical production and discharging power of ES. This value is adjusted by subtracting the FDs capacity, as detailed in constraints (2d) and (2e) [15].

$$\sum_{r\in\mathcal{R}} \left[p_{r,t} + \boldsymbol{r}_{r,t}\right] + \sum_{\theta\in\Theta} \left[p_{\theta,t} + \boldsymbol{r}_{\theta,t}\right] + \sum_{c\in\mathcal{C}} \left[p_{c,t} + \boldsymbol{r}_{c,t}\right] + \sum_{s\in\mathcal{S}} \left[p_{s,t} + \boldsymbol{r}_{s,t}\right] - \sum_{d\in\mathcal{D}} \left[p_{d,t} - \boldsymbol{r}_{d,t}\right] = p_t^{DA} + \boldsymbol{r}_t^{SR}; \quad \forall t \quad (2a)$$

$$p_t^{DA} + r_t^{SR,\uparrow} \le \sum_{r\in\mathcal{R}} \bar{P}_r + \sum_{\theta\in\Theta} \bar{P}_\theta + \sum_{c\in\mathcal{C}} \bar{P}_c + \sum_{s\in\mathcal{S}} \bar{P}_s^{-}; \quad \forall t \quad (2b)$$

$$-\sum_{s\in\mathcal{S}} \bar{P}_s^{+} - \sum_{d\in\mathcal{D}} \bar{P}_d \le p_t^{DA} - r_t^{SR,\downarrow}; \quad \forall t \quad (2c)$$

$$r_t^{SR,\uparrow} \le \kappa \left(\sum_{r\in\mathcal{R}} \bar{P}_r + \sum_{\theta\in\Theta} \bar{P}_\theta + \sum_{c\in\mathcal{C}} \bar{P}_c + \sum_{s\in\mathcal{S}} \bar{P}_s^{-} - \sum_{d\in\mathcal{D}} \bar{P}_d\right); \quad \forall t \quad (2d)$$

$$r_t^{SR,\downarrow} \le \kappa \left(\sum_{r\in\mathcal{R}} \bar{P}_r + \sum_{\theta\in\Theta} \bar{P}_\theta + \sum_{c\in\mathcal{C}} \bar{P}_c + \sum_{s\in\mathcal{S}} \bar{P}_s^{-} - \sum_{d\in\mathcal{D}} \bar{P}_d\right); \quad \forall t \quad (2e)$$

3.1.3. Carbon credit constraints

Building on the approach in [21], the carbon credit constraints are developed to model the temporal interactions across sample days in carbon trading. The number of carbon credits traded by the VPP in each sample day (n_t^{CT}) is defined by equality constraint (3a), which balances

[1] The time set for t is assumed to be $\mathcal{T}$ unless explicitly specified otherwise.

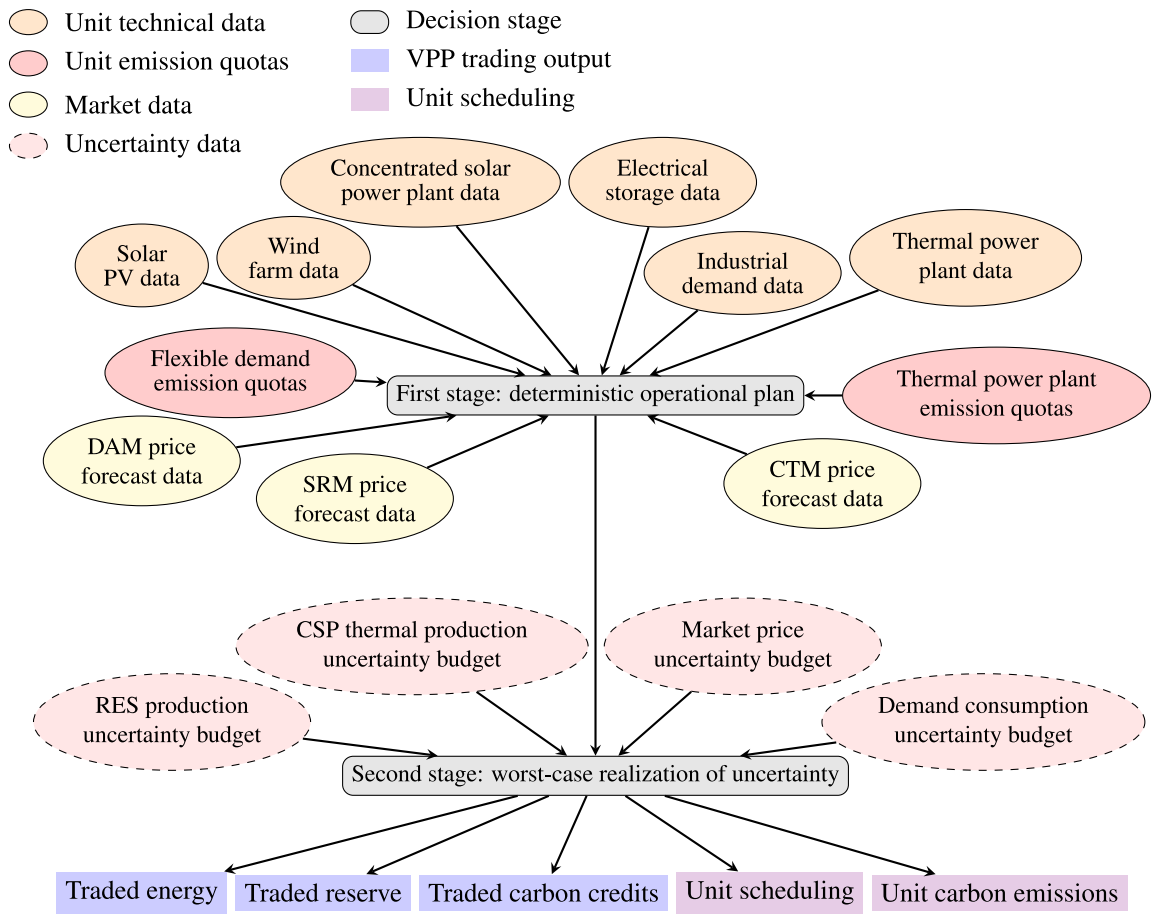

Fig. 2. The interaction among VPP components, various markets, and uncertainty sources in the proposed two-stage RO model.

the saved credits for CO_2 emissions (n_t^{Saved}) and the used credits (n_t^{Used}) from the free allocation. Constraints (3b) and (3c) compute the carbon credits required for electricity production by TPPs and electricity consumption by industrial FDs, respectively. These calculations are based on the total energy and reserve of these units, along with the emission factors α_c and α_d. These factors quantify CO_2 emissions (in tons) per MW for production and consumption. Constraint (3d) calculates the total emissions of VPP units (n^{VPP}), while constraint (3e) ensures that the total saved emissions across all sample days equal the required credits for total emissions. Constraint (3f) defines the CO_2 emission quotas for TPPs and industrial FDs based on their maximum generation and consumption levels, as well as the emission factors ι_c and ι_d. These factors, assigned according to the EU ETS [34], vary depending on the emission intensity of each type of unit. Constraint (3g) enforces that the total used carbon credits across all sample days matches the annual free allocation. Constraints (3h) and (3i) determine the allowable credits per sample day, with constraint (3i) linking the current sample day's allowance to the previous sample day's remaining credits after trades and emissions. Constraints (3j)–(3l) define the buy (n_t^{Buy}) and sell (n_t^{Sell}) variables in the CTM as non-negative and mutually exclusive. This exclusivity is enforced by the binary variable u^{CT}, which prevents simultaneous buying and selling to avoid exploiting carbon price differences between sample days. Finally, constraints (3m) and (3n) show the nature of positive and binary variables, respectively.

$$n_t^{CT} + n_t^{Saved} = n_t^{Used} \; ; \qquad \forall t \in \mathcal{T}^{Day} \quad (3a)$$

$$n_{c,t} = \alpha_c \left(p_{c,t} + r_{c,t}^{\uparrow} \right) \; ; \qquad \forall c, t \quad (3b)$$

$$n_{d,t} = \alpha_d \left(p_{d,t} + r_{d,t}^{\downarrow} \right) \; ; \qquad \forall d, t \quad (3c)$$

$$n^{VPP} = \sum_{t \in \mathcal{T}} \sum_{c \in \mathcal{C}} n_{c,t} + \sum_{t \in \mathcal{T}} \sum_{c \in \mathcal{D}} n_{d,t} \; ; \quad (3d)$$

$$\sum_{t \in \mathcal{T}^{Day}} n_t^{Saved} = n^{VPP} \; ; \quad (3e)$$

$$n^{Allocated} = \sum_{c \in \mathcal{C}} \iota_c \bar{P}_c + \sum_{d \in \mathcal{D}} \iota_d \bar{P}_d \; ; \quad (3f)$$

$$\sum_{t \in \mathcal{T}^{Day}} n_t^{Used} = n^{Allocated} \; ; \quad (3g)$$

$$n_1^{Allowed} = n^{Allocated} \; ; \quad (3h)$$

$$n_t^{Allowed} = n_{t-1}^{Allowed} - n_{t-1}^{CT} - \sum_{c \in \mathcal{C}} n_{c,t-1} - \sum_{d \in \mathcal{D}} n_{d,t-1} \; ; \quad \forall t \in \mathcal{T}^{Day} \backslash \{1\} \quad (3i)$$

$$n_t^{CT} = n_t^{Sell} - n_t^{Buy} \; ; \qquad \forall t \in \mathcal{T}^{Day} \quad (3j)$$

$$n_t^{Sell} \leq M \left(u^{CT} \right) \; ; \qquad \forall t \in \mathcal{T}^{Day} \quad (3k)$$

$$n_t^{Buy} \leq M \left(1 - u^{CT} \right) \; ; \qquad \forall t \in \mathcal{T}^{Day} \quad (3l)$$

$$n_t^{Saved}, n_t^{Used}, n_t^{Sell}, n_t^{Buy} \geq 0 \; ; \qquad \forall t \in \mathcal{T}^{Day} \quad (3m)$$

$$u^{CT} \in \{0, 1\} \; ; \quad (3n)$$

3.1.4. Thermal power plant constraints

Constraints (4a)–(4b) define the upper and lower bounds for the production of each TPP, taking into account the provision of secondary reserve. The binary nature of the variables is indicated in (4c). Appendix B outlines the minimum up and down time requirements for TPPs, based on the approach proposed in [35]. Appendix C presents the reserve provision capability constraints of TPPs.

$$p_{c,t} + r_{c,t}^{\uparrow} \leq \bar{P}_c u_{c,t} \; ; \qquad \forall c, t \quad (4a)$$

$$\underline{P}_c u_{c,t} \le p_{c,t} - r^{\downarrow}_{c,t} \; ; \qquad \forall c,t \qquad (4b)$$

$$u_{c,t} \in \{0,1\} \; ; \qquad \forall c,t \qquad (4c)$$

3.1.5. Electrical storage constraints

A comprehensive formulation for the ESs is presented in (5), developed to integrate both the energy and secondary reserve capabilities of the ES. To have enough energy in case of reserve activation, the model, inspired by [36], assigns a portion of the ES's energy capacity specifically for upward (↑) and downward (↓) secondary reserve provision. Constraints (5a)–(5d) regulate the charging (+) and discharging (−) power of the ES, incorporating the allocation of upward and downward reserves. These constraints allow the ES to provide reserves in both charging and discharging states. The binary variable $u_{s,t}$ indicates the operational state of the ES, with a value of 1 for charging and 0 for discharging. The final values of the upward and downward reserves provided by the ES are calculated based on its reserve contributions during either charging or discharging, as outlined in Eqs. (5e)–(5f). The relationship between the energy and power of the ES, accounting for its charging and discharging efficiencies, is defined by (5g). Additionally, Eq. (5h) ensures that the state of charge remains consistent between the initial and final periods of each sample day. This is crucial for DAM operations and representative period scheduling, as it maintains the ES energy level at the same state at the beginning of each cycle. A fraction of the ES's energy capacity is allocated for upward and downward reserve provision, as specified by the variables $\sigma^{\uparrow}_s$ and $\sigma^{\downarrow}_s$ in (5i)–(5j). Based on this allocated energy, the operational energy limits of the ES are established in (5k). The binary nature of the variable is clarified in (5l).

$$\underline{P}^{+}_s u_{s,t} \le p^{+}_{s,t} - r^{+,\uparrow}_{s,t} \; ; \qquad \forall s,t \qquad (5a)$$

$$p^{+}_{s,t} + r^{+,\downarrow}_{s,t} \le \bar{P}^{+}_s u_{s,t} \; ; \qquad \forall s,t \qquad (5b)$$

$$p^{-}_{s,t} + r^{-,\uparrow}_{s,t} \le \bar{P}^{-}_s \left(1 - u_{s,t}\right) \; ; \qquad \forall s,t \qquad (5c)$$

$$\underline{P}^{-}_s \left(1 - u_{s,t}\right) \le p^{-}_{s,t} - r^{-,\downarrow}_{s,t} \; ; \qquad \forall s,t \qquad (5d)$$

$$r^{\uparrow}_{s,t} = r^{+,\uparrow}_{s,t} + r^{-,\uparrow}_{s,t} \; ; \qquad \forall s,t \qquad (5e)$$

$$r^{\downarrow}_{s,t} = r^{+,\downarrow}_{s,t} + r^{-,\downarrow}_{s,t} \; ; \qquad \forall s,t \qquad (5f)$$

$$e_{s,t} = e_{s,t-1} + p^{+}_{s,t}\eta^{+}_s \Delta t - \frac{p^{-}_{s,t}\Delta t}{\eta^{-}_s} \; ; \qquad \forall s, t\backslash\{1\} \qquad (5g)$$

$$e_{s,1} = e_{s,t=T} \; ; \qquad \forall s \qquad (5h)$$

$$\sum_{t\in\mathcal{T}} \frac{r^{\uparrow}_{s,t}\Delta t}{\eta^{-}_s} \le \sigma^{\uparrow}_s \left(\bar{E}_s - \underline{E}_s\right) \; ; \qquad \forall s \qquad (5i)$$

$$\sum_{t\in\mathcal{T}} r^{\downarrow}_{s,t}\eta^{+}_s \Delta t \le \sigma^{\downarrow}_s \left(\bar{E}_s - \underline{E}_s\right) \; ; \qquad \forall s \qquad (5j)$$

$$\underline{E}_s + \sigma^{\downarrow}_s \left(\bar{E}_s - \underline{E}_s\right) \le e_{s,t} \le \bar{E}_s - \sigma^{\downarrow}_s \left(\bar{E}_s - \underline{E}_s\right) \; ; \qquad \forall s,t \qquad (5k)$$

$$u_{s,t} \in \{0,1\} \; ; \qquad \forall s,t \qquad (5l)$$

3.1.6. Concentrated solar power plant

CSPs are solar power plants that use sunlight to generate thermal energy, which can then be converted into electricity. CSPs employ long, curved mirrors to focus sunlight onto a tube filled with a heat-transfer fluid, which absorbs the heat and enables energy transfer in the Solar Field (SF). The thermal energy is transformed into electrical power within the turbine of the CSP, where steam generated by the heated fluid propels the turbine. Furthermore, molten salt TS allow CSPs to store thermal energy for several hours, enabling electricity generation even after sunset [37]. It is important to note that the TS can only be charged when energy is available at the SF, meaning it cannot be charged by consuming (*purchasing*) energy from the grid as shown in Fig. 1.

The process of converting thermal energy into electrical energy in the turbine of the CSP is formulated in (6) [38]. Constraint (6a) specifies the boundaries for the thermal power output of the SF, considering a fixed value for the uncertain parameter of solar irradiation energy. The thermal power directed to the turbine for electricity generation, as described in (6b), is integrated by multiple factors. These encompass the thermal power provided by the SF, the discharging/charging thermal power of the TS, and the turbine startup losses. The conversion of thermal power to electrical power is achieved by incorporating the turbine's efficiency η_θ. The electrical power and reserve of the CSP are bounded by its maximum and minimum electrical output capacities. These limits also depend on the turbine's commitment status, denoted by the binary variable $u_{\theta,t}$, as detailed in (6c)–(6d). The turbine's commitment status and its related constraints, such as minimum up/down time requirements, outlined in Appendix B. Additionally, the constraints associated with the TS of the CSP mirror those of ES constraints defined in Section 3.1.5. These constraints are excluded here for brevity. Lastly, the nature of the binary variables is defined in accordance with (6e).

$$0 \le p^{SF}_{\theta,t} \le P^{SF}_{\theta,t} \; ; \qquad \forall \theta,t \qquad (6a)$$

$$\frac{p_{\theta,t}}{\eta_\theta} = p^{SF}_{\theta,t} + p^{TS,-}_{\theta,t} - p^{TS,+}_{\theta,t} - K_\theta v^{SU}_{\theta,t} \bar{P}_\theta \; ; \qquad \forall \theta,t \qquad (6b)$$

$$p_{\theta,t} + r^{\uparrow}_{\theta,t} \le \bar{P}_\theta u_{\theta,t} \; ; \qquad \forall \theta,t \qquad (6c)$$

$$\underline{P}_\theta u_{\theta,t} \le p_{\theta,t} - r^{\downarrow}_{\theta,t} \; ; \qquad \forall \theta,t \qquad (6d)$$

$$u_{\theta,t}, v^{SU}_{\theta,t} \in \{0,1\} \; ; \qquad \forall \theta,t \qquad (6e)$$

3.1.7. RES constraints

The constraints governing RES are formulated in (7). Constraints (7a) and (7b) define the maximum and minimum limits for the energy output and reserve of RES, respectively, based on the precise value of the uncertain parameter. Notably, RES, such as WFs and solar PVs, have the ability to contribute to secondary reserve provision, contingent on their technical capabilities [39,40]. Upward reserve is feasible when RES are operated below their full capacity and can ramp up generation during secondary reserve activation. On the other hand, downward reserve is facilitated by reducing their output power from the current operating level.

$$p_{r,t} + r^{\uparrow}_{r,t} \le P_{r,t} \; ; \qquad \forall r,t \qquad (7a)$$

$$\underline{P}_r \le p_{r,t} - r^{\downarrow}_{r,t} \; ; \qquad \forall r,t \qquad (7b)$$

3.1.8. Flexible demand constraints

The constraints for FDs are outlined in (8), following the approach in [38]. Constraint (8a) establishes the minimum limit for FDs in each time period, based on predefined demand profiles and fixed values for the uncertainties within each profile. Constraint (8b) ensures that only one demand profile is selected by the algorithm from multiple available profiles. The allowable range for FDs, including reserve provision, is defined by the lower and upper bounds in (8c) and (8d), respectively. FDs are permitted a specific percentage of flexibility relative to their predefined profiles, which is allocated for upward and downward reserve provision as defined in (8e) and (8f), respectively. Additionally, the minimum energy consumption over the time horizon (sample day) for FDs is assigned by (8g).

$$p_{d,t} \ge \sum_{m\in\mathcal{M}} \left[P_{d,m,t} u_{d,m}\right] \; ; \qquad \forall d,t \qquad (8a)$$

$$\sum_{m\in\mathcal{M}} u_{d,m} = 1 \; , \qquad \forall d \qquad (8b)$$

$$\underline{P}_d \le p_{d,t} - r^{\uparrow}_{d,t} \; ; \qquad \forall d,t \qquad (8c)$$

$$p_{d,t} + r^{\downarrow}_{d,t} \le \bar{P}_d \; ; \qquad \forall d,t \qquad (8d)$$

$$r^{\uparrow}_{d,t} \le \underline{\beta}_{d,t} p_{d,t} \; ; \qquad \forall d,t \qquad (8e)$$

$$r^{\downarrow}_{d,t} \le \bar{\beta}_{d,t} p_{d,t} \; ; \qquad \forall d,t \qquad (8f)$$

$$\underline{E}_d \le \sum_{t\in\mathcal{T}} \left[p_{d,t}\Delta t - r^{\uparrow}_{d,t} \right] \; ; \qquad \forall d \qquad (8g)$$

3.1.9. Remarks

The optimization problem outlined in (1)–(8) represents a deterministic model for VPP participation in the DAM and SRM, as well as for CTM. In the following section, the proposed formulation is extended to integrate various uncertainties, including electricity prices, production from RES and CSPs, and consumption of FDs, into the optimization framework.

3.2. Robust formulation

The deterministic formulation discussed in Section 3.1 does not consider the fluctuations of uncertain parameters. However, uncertainties in DAM, SRM, and CTM prices can have negative (or positive) effects on the VPP profit. Moreover, uncertainties in the production of RES and CSP and consumption of FD can result in reduced generation or higher demand, thereby influencing the VPP market profits. Consequently, the VPP operator must incorporate the impact of these uncertainties into its decision-making process. The following section extends the optimization problem to incorporate the effects of uncertainties on the VPP's scheduling and bidding strategy. In this regard, a flexible two-stage RO strategy is formulated by expanding the RO theory introduced in [41].

3.2.1. Two-stage robust model

A two-stage RO model is developed in (9) to address multiple uncertain parameters within the optimization framework. In the first stage, the VPP operator aims to maximize its objective function (9a), which mirrors the deterministic objective function (1). In the second stage, uncertainties negatively influence the electricity prices in the DAM, SRM and CTM. This is formulated as a minimization problem for the uncertainty set of variables $\{\lambda^{DA}_t, \lambda^{SR,\uparrow}_t, \lambda^{SR,\downarrow}_t, \lambda^{CT}_t\}$. Furthermore, uncertainties are modeled to potentially reduce the electrical output of RES and the thermal output of CSPs, while increasing the consumption of FDs, as expressed in constraints (9b)–(9d). The decision variables of these uncertainties are represented by the set $\{P_{r,t}, P^{SF}_{\theta,t}, P_{d,t}\}$ (with index m of uncertain parameter $P_{d,m,t}$ in (8a) omitted for simplicity). Notably, unlike the deterministic formulation, the uncertainty sets $\{\lambda^{DA}_t, \lambda^{SR,\uparrow}_t, \lambda^{SR,\downarrow}_t, \lambda^{CT}_t\}$ and $\{P_{r,t}, P^{SF}_{\theta,t}, P_{d,t}\}$ now include second-stage decision variables, which were treated as fixed parameters in the deterministic model. Constraints from the deterministic problem in Section 3.1 that remain unaffected by uncertainties are retained and defined in (9e).

$$\begin{aligned}
&\max_{\Xi^{DA+SR+CT}} \left\{ \min_{\{\lambda^{DA}_t, \lambda^{SR,\uparrow}_t, \lambda^{SR,\downarrow}_t, \lambda^{CT}_t\}} \left\{ \sum_{t\in\mathcal{T}} \lambda^{DA}_t p^{DA}_t \Delta t \right.\right. \\
&+ \sum_{t\in\mathcal{T}} \left[\lambda^{SR,\uparrow}_t r^{SR,\uparrow}_t + \lambda^{SR,\downarrow}_t r^{SR,\downarrow}_t \right] + \sum_{t\in\mathcal{T}^{Day}} \lambda^{CT}_t n^{CT}_t \\
&- \sum_{t\in\mathcal{T}} \sum_{r\in\mathcal{R}} C_r p_{r,t}\Delta t - \sum_{t\in\mathcal{T}} \sum_{\theta\in\Theta} C_\theta p_{\theta,t}\Delta t \\
&\left.\left. - \sum_{t\in\mathcal{T}} \sum_{c\in\mathcal{C}} \left[C_c p_{c,t}\Delta t + C^{SU}_c v^{SU}_{c,t} + C^{SD}_c v^{SD}_{c,t} \right] - \sum_{t\in\mathcal{T}} \sum_{s\in\mathcal{S}} M_s \frac{C_s}{\bar{E}_s} p_{s,t}\Delta t \right\} \right\} \qquad (9a)
\end{aligned}$$

st.

$$p_{r,t} + r^{\uparrow}_{r,t} \le \min_{P_{r,t}} \{P_{r,t}\} \; ; \qquad \forall r,t \qquad (9b)$$

$$p^{SF}_{\theta,t} \le \min_{P^{SF}_{\theta,t}} \left\{ P^{SF}_{\theta,t} \right\} \; ; \qquad \forall \theta,t \qquad (9c)$$

$$p_{d,t} \ge -\min_{P_{d,t}} \{-P_{d,t}\} \; ; \qquad \forall d,t \qquad (9d)$$

(2)–(5), (6b)–(6e), (7b), (8b)–(8g); (9e)

Flexibility in handling uncertainty is achieved through the *uncertainty budget* parameter. This parameter is applied to uncertain parameters in the DAM, SRM, and CTM prices (i.e., Γ^{DA}, $\Gamma^{SR,\uparrow}$, $\Gamma^{SR,\downarrow}$, and Γ^{CT}). It is also applied to uncertain parameters of the production of RES and CSPs and the consumption of FDs (Γ_r, Γ_θ, and Γ_d). For short-term uncertainties – such as DAM/SRM prices, RES output, and demand – the uncertainty budget is defined as an integer parameter ranging from 0 to 24 across the hours of each sample day. For long-term uncertainties, such as CTM prices, the budget represents the number of sample days subject to worst-case values and ranges from 0 to 4. By adjusting these uncertainty budgets, the VPP operator can vary the level of conservatism in decision-making, from optimistic to pessimistic. In mathematical terms, the uncertainty budget specifies how many time intervals allowed to deviate from predicted values for uncertain parameters. A smaller budget reflects a more optimistic outlook with limited variability, whereas a larger budget results in a more conservative approach by accounting for a wider range of possible fluctuations. For example, for the DAM price uncertainty, the asymmetric uncertainty bound is defined as $\lambda^{DA}_t \in \left[\tilde{\lambda}^{DA}_t - \check{\lambda}^{DA}_t, \tilde{\lambda}^{DA}_t + \hat{\lambda}^{DA}_t\right]$, where, in general, $\check{\lambda}^{DA}_t \neq \hat{\lambda}^{DA}_t$. Within this bound, the worst-case DAM prices depend on the direction of the VPP's energy trades in a given period. Specifically, the minimum price represents the worst case when the VPP is selling energy, while the maximum price represents the worst case when the VPP is buying energy. For the CTM price uncertainty, an asymmetric uncertainty bound similar to that of the DAM price is defined as $\lambda^{CT}_t \in \left[\tilde{\lambda}^{CT}_t - \check{\lambda}^{CT}_t, \tilde{\lambda}^{CT}_t + \hat{\lambda}^{CT}_t\right]$, where, in general, $\check{\lambda}^{CT}_t \neq \hat{\lambda}^{CT}_t$. For the uncertainty bounds of up/down SRM prices $\left(\lambda^{SR,\uparrow}_t \in \left[\tilde{\lambda}^{SR,\uparrow}_t - \check{\lambda}^{SR,\uparrow}_t, \hat{\lambda}^{SR,\uparrow}_t\right]\right.$ and $\left.\lambda^{SR,\downarrow}_t \in \left[\tilde{\lambda}^{SR,\downarrow}_t - \check{\lambda}^{SR,\downarrow}_t, \hat{\lambda}^{SR,\downarrow}_t\right]\right)$, only negative deviations are considered. The same applies to the electrical production of RES $\left(P_{r,t} \in \left[\tilde{P}_{r,t} - \check{P}_{r,t}, \hat{\tilde{P}}_{r,t}\right]\right)$ and the thermal production of CSPs $\left(P^{SF}_{\theta,t} \in \left[\tilde{P}^{SF}_{\theta,t} - \check{P}^{SF}_{\theta,t}, \hat{\tilde{P}}^{SF}_{\theta,t}\right]\right)$. Conversely, for FDs $\left(P_{d,t} \in \left[\check{\tilde{P}}_{d,t}, \check{\tilde{P}}_{d,t} + \hat{P}_{d,t}\right]\right)$, only positive deviations are taken into account. This ensures that the worst-case periods, aligned with the VPP operator's chosen strategy or level of conservatism via the uncertainty budgets, is accurately reflected in the optimization problem. Deviations in the opposite direction would typically lead to higher profits for the VPP, which is not the focus of this modeling approach.

The objective function (10a) incorporates the predefined bounds of uncertain parameters related to DAM, SRM, and CTM prices. The lower-level maximization problem in (10a) identifies the worst-case periods for VPP profit by considering fluctuations in different prices due to uncertainty. To model the worst-case periods, the time period sets $\mathcal{T}^{DA}$, $\mathcal{T}^{SR,\uparrow}$, $\mathcal{T}^{SR,\downarrow}$, and $\mathcal{T}^{CT}$ are introduced. These sets denote the periods (or sample days for CTM price) in which price deviations from the median or upper bound exert the greatest adverse impact on the VPP's profit. The VPP operator can adjust the level of conservatism by controlling the time period sets $\mathcal{T}^{DA}$, $\mathcal{T}^{SR,\uparrow}$, $\mathcal{T}^{SR,\downarrow}$, and $\mathcal{T}^{CT}$ using the uncertainty budgets Γ^{DA}, $\Gamma^{SR,\uparrow}$, $\Gamma^{SR,\downarrow}$, and Γ^{CT}. Since the operational costs of VPP units, and the VPP's profit for median values of DAM and CTM prices and the upper bound of SRM prices are unaffected by these uncertainties, the corresponding terms can be shifted to the upper-level problem. Furthermore, the auxiliary variables $z_t{}^{DA}$ and $z_t{}^{CT}$ in (10a) represent the energy traded in the DAM and the carbon credits traded in the CTM, respectively. The variables $z_t{}^{DA}$ and $z_t{}^{CT}$ are constrained by (10b) and (10c), respectively. These constraints effectively captures the asymmetric nature of price uncertainties based on the direction of energy traded in the DAM and carbon credits traded in the CTM. Eqs. (10d)–(10f) model the uncertainties in the electrical production of RES, thermal production of CSPs, and consumption of FDs, respectively. These constraints are formulated by integrating the defined uncertainty bounds for the worst-case periods $\mathcal{T}_r$, $\mathcal{T}_\theta$, and $\mathcal{T}_d$. For instance, in constraint (10d), the worst-case deviation in electrical power due to uncertainty, $\check{P}_{r,t'}$, is subtracted from the upper bound of the forecasted

value $\hat{\hat{P}}_{r,t}$. This subtraction is applied only when t' corresponds to period t and is part of the set $\mathcal{T}_r$ (i.e., $t' \in \mathcal{T}_r, t' = t$). The positive nature of the auxiliary variables is ensured in (10g), while constraint (10h) outlines the deterministic constraints.

$$\max_{\Xi^{DA+SR+CT}} \left\{ \sum_{t\in\mathcal{T}} \tilde{\lambda}_t^{DA} p_t^{DA} \Delta t + \sum_{t\in\mathcal{T}} \left[\hat{\tilde{\lambda}}_t^{SR,\uparrow} r_t^{SR,\uparrow} + \hat{\tilde{\lambda}}_t^{SR,\downarrow} r_t^{SR,\downarrow} \right] + \sum_{t\in\mathcal{T}^{Day}} \tilde{\lambda}_t^{CT} n_t^{CT} \right.$$
$$- \sum_{t\in\mathcal{T}} \sum_{r\in\mathcal{R}} C_r p_{r,t} \Delta t - \sum_{t\in\mathcal{T}} \sum_{\theta\in\Theta} C_\theta p_{\theta,t} \Delta t$$
$$- \sum_{t\in\mathcal{T}} \sum_{c\in\mathcal{C}} \left[C_c p_{c,t} \Delta t + C_c^{SU} v_{c,t}^{SU} + C_c^{SD} v_{c,t}^{SD} \right] - \sum_{t\in\mathcal{T}} \sum_{s\in\mathcal{S}} M_s \frac{C_s}{E_s} p_{s,t} \Delta t$$
$$- \max_{\left\{ \begin{array}{l} \mathcal{T}^{DA}, \\ \mathcal{T}^{SR,\uparrow}, \\ \mathcal{T}^{SR,\downarrow}, \\ \mathcal{T}^{CT} \end{array} \middle| \begin{array}{l} |\mathcal{T}^{DA}| = \Gamma^{DA}, \\ |\mathcal{T}^{SR,\uparrow}| = \Gamma^{SR,\uparrow}, \\ |\mathcal{T}^{SR,\downarrow}| = \Gamma^{SR,\downarrow}, \\ |\mathcal{T}^{CT}| = \Gamma^{CT} \end{array} \right\}} \left\{ \sum_{t\in\mathcal{T}^{DA}} \check{\lambda}_t^{DA} z_t^{DA} + \sum_{t\in\mathcal{T}^{SR,\uparrow}} \check{\lambda}_t^{SR,\uparrow} r_t^{SR,\uparrow} \right.$$
$$\left. \left. + \sum_{t\in\mathcal{T}^{SR,\downarrow}} \check{\lambda}_t^{SR,\downarrow} r_t^{SR,\downarrow} + \sum_{t\in\mathcal{T}^{CT}} \check{\lambda}_t^{CT} z_t^{CT} \right\} \right\} \tag{10a}$$

st.

$$-\frac{\check{\lambda}_t^{DA}}{\hat{\lambda}_t^{DA}} z_t^{DA} \le p_t^{DA} \Delta t \le z_t^{DA} \; ; \qquad \forall t \in \mathcal{T}^{DA} \tag{10b}$$

$$-\frac{\check{\lambda}_t^{CT}}{\hat{\lambda}_t^{CT}} z_t^{CT} \le n_t^{CT} \le z_t^{CT} \; ; \qquad \forall t \in \mathcal{T}^{CT} \tag{10c}$$

$$p_{r,t} + r_{r,t}^{\uparrow} \le \hat{\tilde{P}}_{r,t} - \max_{\{\mathcal{T}_r | \, |\mathcal{T}_r| = \Gamma_r\}} \left\{ \sum_{t'\in\mathcal{T}_r, t'=t} \check{P}_{r,t'} \right\} \; ; \qquad \forall r, t \tag{10d}$$

$$p_{\theta,t}^{SF} \le \hat{\tilde{P}}_{\theta,t}^{SF} - \max_{\{\mathcal{T}_\theta | \, |\mathcal{T}_\theta| = \Gamma_\theta\}} \left\{ \sum_{t'\in\mathcal{T}_\theta, t'=t} \check{P}_{\theta,t'}^{SF} \right\} \; ; \qquad \forall \theta, t \tag{10e}$$

$$p_{d,t} \ge \check{\tilde{P}}_{d,t} + \max_{\{\mathcal{T}_d | \, |\mathcal{T}_d| = \Gamma_d\}} \left\{ \sum_{t'\in\mathcal{T}_d, t'=t} \hat{P}_{d,t'} \right\} \; ; \qquad \forall d, t \tag{10f}$$

$$z_t^{DA}, z_t^{CT} \ge 0 \; ; \qquad \forall t \tag{10g}$$

(2)–(5), (6b)–(6e), (7b), (8b)–(8g); (10h)

3.2.2. Inner problems reformulation

Although the protection function in (10a) (the maximization term in the lower level of the objective function) represents the worst-case periods for uncertain parameters, the selection of values based on the defined sets can be formulated linearly. To achieve this, Proposition 1 from [41] is applied. Given the optimal values (denoted by the superscript *) of the upper-level variables $z_t^{DA^*}$, $r_t^{SR,\uparrow^*}$, $r_t^{SR,\downarrow^*}$, and $z_t^{CT^*}$, the linear problem (11) is equivalent to the protection function in (10a). Constraints (11b)–(11e) define the bounds for the auxiliary variables w_t^{DA}, $w_t^{SR,\uparrow}$, $w_t^{SR,\downarrow}$, and w_t^{CT}. These constraints correspond to the uncertain parameters of DAM, SRM, and CTM prices and are based on their respective uncertainty budgets Γ^{DA}, $\Gamma^{SR,\uparrow}$, $\Gamma^{SR,\downarrow}$, and Γ^{CT}. Constraints (11f)–(11i) ensure that the positive auxiliary variables w_t^{DA}, $w_t^{SR,\uparrow}$, $w_t^{SR,\downarrow}$, and w_t^{CT} do not exceed their limits. This preserves the same optimal value for the objective function in (11a) as the protection function in (10a). Additionally, dual variables for each constraint are introduced to derive the final MILP formulation.

$$\max \left\{ \sum_{t\in\mathcal{T}^{DA}} \check{\lambda}_t^{DA} z_t^{DA^*} w_t^{DA} + \sum_{t\in\mathcal{T}^{SR,\uparrow}} \check{\lambda}_t^{SR,\uparrow} r_t^{SR,\uparrow^*} w_t^{SR,\uparrow} \right.$$
$$\left. + \sum_{t\in\mathcal{T}^{SR,\downarrow}} \check{\lambda}_t^{SR,\downarrow} r_t^{SR,\downarrow^*} w_t^{SR,\downarrow} + \sum_{t\in\mathcal{T}^{CT}} \check{\lambda}_t^{CT} z_t^{CT^*} w_t^{CT} \right\} \tag{11a}$$

st.

$$\sum_{t\in\mathcal{T}^{DA}} w_t^{DA} \le \Gamma^{DA} : \delta^{DA} \; ; \tag{11b}$$

$$\sum_{t\in\mathcal{T}^{SR,\uparrow}} w_t^{SR,\uparrow} \le \Gamma^{SR,\uparrow} : \delta^{SR,\uparrow} \; ; \tag{11c}$$

$$\sum_{t\in\mathcal{T}^{SR,\downarrow}} w_t^{SR,\downarrow} \le \Gamma^{SR,\downarrow} : \delta^{SR,\downarrow} \; ; \tag{11d}$$

$$\sum_{t\in\mathcal{T}^{CT}} w_t^{CT} \le \Gamma^{CT} : \delta^{CT} \; ; \tag{11e}$$

$$0 \le w_t^{DA} \le 1 : \psi_t^{DA} \; ; \qquad \forall t \in \mathcal{T}^{DA} \tag{11f}$$

$$0 \le w_t^{SR,\uparrow} \le 1 : \psi_t^{SR,\uparrow} \; ; \qquad \forall t \in \mathcal{T}^{SR,\uparrow} \tag{11g}$$

$$0 \le w_t^{SR,\downarrow} \le 1 : \psi_t^{SR,\downarrow} \; ; \qquad \forall t \in \mathcal{T}^{SR,\downarrow} \tag{11h}$$

$$0 \le w_t^{CT} \le 1 : \psi_t^{CT} \; ; \qquad \forall t \in \mathcal{T}^{CT} \tag{11i}$$

The protection function of electrical production uncertainty in RES in constraint (10d), is presented as the linear formulation (12). The objective function (12a) maximizes the deviation in electrical production caused by uncertainty during the corresponding period t ($t' \in \mathcal{T}_r$, $t' = t$) in (12b). The sum of the auxiliary positive variables $w_{r,t'}$ for the corresponding period t and other worst-case periods, which are fixed at their optimal values, is constrained by the uncertainty budget Γ_r. The bound for the auxiliary variable $w_{r,t'}$ is specified in (12c). It is important to note that the linear formulation (12) accounts for the temporal constraints of the uncertain parameter across all time periods of each sample day. This contrasts with the approach in [3], which defines the worst-case value of the uncertain parameter within a single period. This approach enables the VPP to adjust a single uncertain parameter for each sample day, rather than managing multiple parameters for each time period and uncertain parameter.

The equivalent linear formulations for selecting the worst-case periods in constraints (10e)–(10f), which address uncertainties in CSPs thermal production and FDs consumption, respectively, can be derived in a manner similar to (12). These formulations are provided in Appendix D.

$$\max \sum_{t'\in\mathcal{T}_r, t'=t} \check{P}_{r,t'} w_{r,t'} \; ; \qquad \forall r, t \tag{12a}$$

st.

$$\sum_{t'\in\mathcal{T}_r, t'=t} w_{r,t'} + \sum_{t'\in\mathcal{T}_r, t'\ne t} w_{r,t'}^* \le \Gamma_r : \delta_r \; ; \tag{12b}$$

$$0 \le w_{r,t'} \le 1 : \psi_{r,t'} \; ; \qquad \forall t' \in \mathcal{T}_r, t' = t \tag{12c}$$

3.2.3. MILP formulation

By leveraging strong duality [42] on the linear formulation in (11), its dual problem can be substituted in place of the protection function in the objective function (10a). Similarly, the protection functions in constraints (10d)–(10f) are replaced with their dual formulations, leading to the final MILP problem in (13). The first to third lines of the objective function (13a) represent the deterministic components. The fourth and fifth lines account for the adverse effects of uncertainties in the DAM, SRM, and CTM prices. Constraints (13b) and (13c) model the asymmetric deviations of DAM and CTM price uncertainty, respectively. The dual constraints of the linear problem (11) are expressed in Constraints (13d)–(13g). Constraint (13h) defines the upper limit for the electrical production of RES while incorporating uncertainty. Since the term $\Gamma_r - \sum_{t'\in\mathcal{T}_r, t'\ne t} w_{r,t'}^*$ in (12b) can only take a value of zero or one, depending on the number of worst-case periods in its defined set, a new binary variable $\chi_{r,t}$ is introduced to represent these conditions. Additionally, a new positive auxiliary variable $z_{r,t}$ is defined in (13h). It is constrained in (13i) using the big-M method [42] to represent the dual term $\chi_{r,t}\delta_r + \psi_{r,t}$. Constraint (13j) represents the dual constraint of the linear problem associated with RES electrical production uncertainty in (12). Constraint (13k) determines the uncertainty budget for the electrical production of RES. Constraints (13l)–(13o) address the CSPs thermal production uncertainty, while constraints (13p)–(13s) handle the FDs consumption uncertainty. These constraints are structured similarly to the electrical production uncertainty constraints for

RES in (13h)–(13k). The key distinction is that, for FDs, the worst-case uncertainty leads to an increase in these parameters, whereas for RES electrical production and CSPs thermal production, it results in a decrease. The nature of the positive and binary variables is specified in (13t)–(13v), and the deterministic constraints are declared in (13w).

It is important to highlight that the refined MILP problem in (13) is designed to flexibly incorporate uncertainties in both the objective function and constraints. This is achieved by adjusting the uncertainty budget defined for temporal constraints. Section 4 presents multiple case studies that thoroughly evaluate the proposed approach in terms of its computational efficiency and ability to manage varying levels of uncertainty.

$$\max_{\Xi^{DA+SR+CT}} \Bigg\{ \sum_{t\in\mathcal{T}} \tilde{\lambda}_t^{DA} p_t^{DA} \Delta t + \sum_{t\in\mathcal{T}} \left[\hat{\tilde{\lambda}}_t^{SR,\uparrow} r_t^{SR,\uparrow} + \hat{\tilde{\lambda}}_t^{SR,\downarrow} r_t^{SR,\downarrow} \right] + \sum_{t\in\mathcal{T}^{Day}} \tilde{\lambda}_t^{CT} n_t^{CT}$$
$$- \sum_{t\in\mathcal{T}} \sum_{r\in\mathcal{R}} C_r p_{r,t} \Delta t - \sum_{t\in\mathcal{T}} \sum_{\theta\in\Theta} C_\theta p_{\theta,t} \Delta t - \sum_{t\in\mathcal{T}} \sum_{c\in\mathcal{C}} \left[C_c p_{c,t} \Delta t + C_c^{SU} v_{c,t}^{SU} + C_c^{SD} v_{c,t}^{SD} \right]$$
$$- \sum_{t\in\mathcal{T}} \sum_{s\in\mathcal{S}} M_s \frac{C_s}{E_s} p_{s,t} \Delta t$$
$$- \Gamma^{DA} \delta^{DA} - \sum_{t\in\mathcal{T}} \psi_t^{DA} - \Gamma^{SR,\uparrow} \delta^{SR,\uparrow} - \Gamma^{SR,\downarrow} \delta^{SR,\downarrow} - \sum_{t\in\mathcal{T}} \left[\psi_t^{SR,\uparrow} + \psi_t^{SR,\downarrow} \right]$$
$$- \Gamma^{CT} \delta^{CT} - \sum_{t\in\mathcal{T}^{Day}} \psi_t^{CT} \Bigg\} \tag{13a}$$

st.

$$- \frac{\check{\lambda}_t^{DA}}{\hat{\lambda}_t^{DA}} z_t^{DA} \le p_t^{DA} \Delta t \le z_t^{DA} \; ; \qquad \forall t \tag{13b}$$

$$- \frac{\check{\lambda}_t^{CT}}{\hat{\lambda}_t^{CT}} z_t^{CT} \le n_t^{CT} \le z_t^{CT} \; ; \qquad \forall t \in \mathcal{T}^{Day} \tag{13c}$$

$$\delta^{DA} + \psi_t^{DA} \ge \check{\lambda}_t^{DA} z_t^{DA} \; ; \qquad \forall t \tag{13d}$$

$$\delta^{SR,\uparrow} + \psi_t^{SR,\uparrow} \ge \check{\lambda}_t^{SR,\uparrow} r_t^{SR,\uparrow} \; ; \qquad \forall t \tag{13e}$$

$$\delta^{SR,\downarrow} + \psi_t^{SR,\downarrow} \ge \check{\lambda}_t^{SR,\downarrow} r_t^{SR,\downarrow} \; ; \qquad \forall t \tag{13f}$$

$$\delta^{CT} + \psi_t^{CT} \ge \check{\lambda}_t^{CT} z_t^{CT} \; ; \qquad \forall t \in \mathcal{T}^{Day} \tag{13g}$$

$$p_{r,t} + r_{r,t}^{\uparrow} \le \hat{\tilde{P}}_{r,t} - \chi_{r,t} \delta_r - \psi_{r,t} = \hat{\tilde{P}}_{r,t} - z_{r,t} \; ; \qquad \forall r,t \tag{13h}$$

$$\delta_r + \psi_{r,t} - M(1-\chi_{r,t}) \le z_{r,t} \le M \chi_{r,t} \; ; \qquad \forall r,t \tag{13i}$$

$$\delta_r + \psi_{r,t} \ge \check{P}_{r,t} \; ; \qquad \forall r,t \tag{13j}$$

$$\sum_t \chi_{r,t} = \Gamma_r \; ; \qquad \forall r \tag{13k}$$

$$p_{\theta,t}^{SF} \le \hat{\tilde{P}}_{\theta,t}^{SF} - \chi_{\theta,t} \delta_\theta - \psi_{\theta,t} = \hat{\tilde{P}}_{\theta,t}^{SF} - z_{\theta,t} \; ; \qquad \forall \theta,t \tag{13l}$$

$$\delta_\theta + \psi_{\theta,t} - M(1-\chi_{\theta,t}) \le z_{\theta,t} \le M \chi_{\theta,t} \; ; \qquad \forall \theta,t \tag{13m}$$

$$\delta_\theta + \psi_{\theta,t} \ge \check{P}_{\theta,t} \; ; \qquad \forall \theta,t \tag{13n}$$

$$\sum_t \chi_{\theta,t} = \Gamma_\theta \; ; \qquad \forall \theta \tag{13o}$$

$$p_{d,t} \ge \check{\tilde{P}}_{d,t} + \chi_{d,t} \delta_d + \psi_{d,t} = \check{\tilde{P}}_{d,t} + z_{d,t} \; ; \qquad \forall d,t \tag{13p}$$

$$\delta_d + \psi_{d,t} - M(1-\chi_{d,t}) \le z_{d,t} \le M \chi_{d,t} \; ; \qquad \forall d,t \tag{13q}$$

$$\delta_d + \psi_{d,t} \ge \hat{P}_{d,t} \; ; \qquad \forall d,t \tag{13r}$$

$$\sum_t \chi_{d,t} = \Gamma_d \; ; \qquad \forall d \tag{13s}$$

$$\delta^{DA}, \delta^{SR,\uparrow}, \delta^{SR,\downarrow}, \delta^{CT}, \psi_t^{DA}, \psi_t^{SR,\uparrow}, \psi_t^{SR,\downarrow}, \psi_t^{CT}, z_t^{DA}, z_t^{CT} \ge 0 \; ; \qquad \forall t \tag{13t}$$

$$\delta_r, \delta_\theta, \delta_d, \psi_{r,t}, \psi_{\theta,t}, \psi_{d,t}, z_{r,t}, z_{\theta,t}, z_{d,t} \ge 0 \; ; \qquad \forall r,\theta,d,t \tag{13u}$$

$$\chi_{r,t}, \chi_{\theta,t}, \chi_{d,t} \in \{0,1\} \; ; \qquad \forall r,\theta,d,t \tag{13v}$$

(2)–(5), (6b)–(6e), (7b), (8b)–(8g); (13w)

3.2.4. Uncertainty bounds estimation

Uncertainty bounds for uncertain parameters can be established using different techniques. Common approaches include analyzing historical datasets that contain observational and measurement information. Other techniques involve applying parametric distributions to characterize uncertainty and utilizing resampling methods such as bootstrapping [43]. Historical data, derived from prior measurements and observations, serves as a valuable resource for uncovering trends and statistical relationships. The approach adopted in this study for setting uncertainty bounds is illustrated in Fig. 3. Specifically, a one-year dataset is compiled for each uncertain parameter, and the values are analyzed on an hourly basis. The four sample days are constructed based on this historical data to reflect typical seasonal characteristics of the uncertain parameters. For each hour, the median, along with the 20th and 80th percentiles, is calculated to represent the central tendency and the lower and upper bounds, respectively. This percentile-based method helps avoid overly conservative estimates while still capturing the typical range of variation. These statistical bounds serve as the foundation for the RO approach, where constructed sample days represent typical seasonal behavior, instead of using data from specific historical calendar days.

Algorithm 1 MILP model workflow for VPP participation in the DAM, SRM, and CTM.

1: **Input:** Technical data of units; emission quotas; market data; uncertain data including forecasted generation profiles (RES, CSP); FD consumption; and DAM, SRM, and CTM prices.
2: **Initialize:** Model parameters; decision variables related to DAM, SRM, and CTM.
3: **Formulate MILP:**
4: • **Objective function:** Maximize the VPP's revenue minus operational costs, including:
5: – Revenue from electricity trading in DAM and SRM
6: – Revenue from carbon credit trading in the CTM
7: – Operational costs of RES, CSP, and TPP
8: – Operational and degradation costs of ES
9: • **Subject to:**
10: – Supply–demand balance constraints
11: – Carbon credit constraints
12: – Technical constraints of units (RES, CSP, TPP, ES, and FD)
13: – Uncertainty constraints related to market prices (DAM, SRM, CTM)
14: – Uncertainty constraints related to unit operation (e.g., RES and CSP production, FD consumption)
15: **Solve:** Use an MILP solver (e.g., CPLEX) to obtain the optimal solution.
16: **Output:** VPP energy and reserve trade results; carbon trading outcomes; unit schedules; carbon emissions; and detailed cost and profit breakdowns.

3.2.5. Model workflow summary

The overall modeling workflow is summarized in Algorithm 1, which outlines the inputs, optimization structure, and outputs of the MILP formulation. It illustrates the role of technical and market data in defining the optimization problem and provides a high-level view of the model's process for determining optimal scheduling, market participation, and emissions trading decisions for the VPP.

4. Case studies

This section outlines the simulation outcomes of the proposed RO model applied to the DAM, SRM, and CTM. The simulations are carried out on a VPP that includes a WF, a solar PV plant, a CSP equipped with TS, a TPP, a Li-ion ES, and an industrial FD. Forecast bounds for the electrical output of the WF and solar PV, along with the thermal output of the CSP, are shown in Fig. 4 for four sample days. These bounds are generated using the methodology in Section 3.2.4. Historical data from CIEMAT Spain [44] is used for solar PV and CSP, and from Iberdrola Spain [45] for the WF. Each sample day represents a season and is weighted equally with the other sample days. Both the WF and solar PV plant have nominal capacities of 50 MW, with respective operating costs of 15 €/MWh and 10 €/MWh. The technical specifications of the CSP are detailed in Table 2, based on data also from [44], and it incurs an operating cost of 25 €/MWh. All unit operating costs have been levelised according to the estimated project costs of various generation

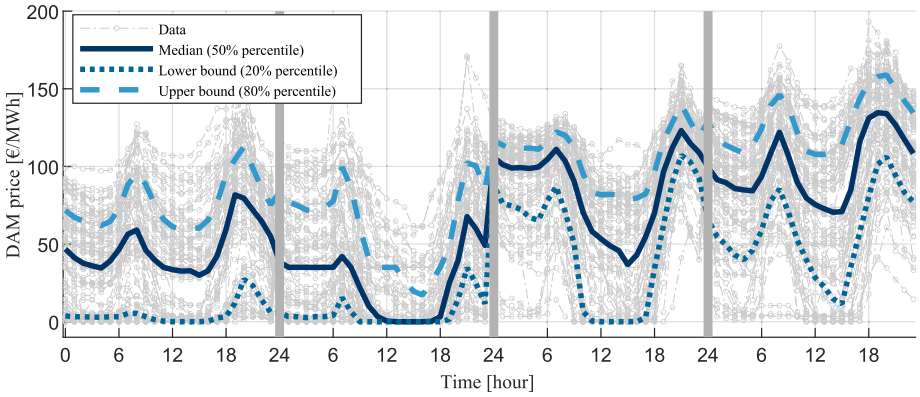

Fig. 3. Using historical data to establish the bound of uncertain parameters.

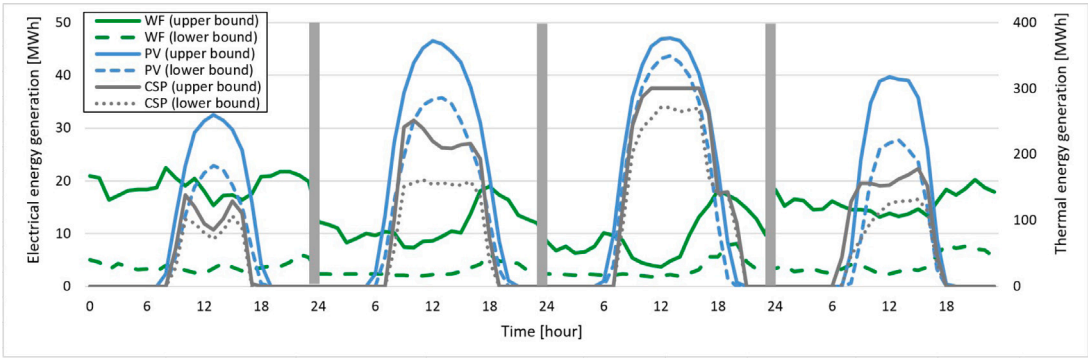

Fig. 4. The forecast bounds of WF, solar PV, and CSP.

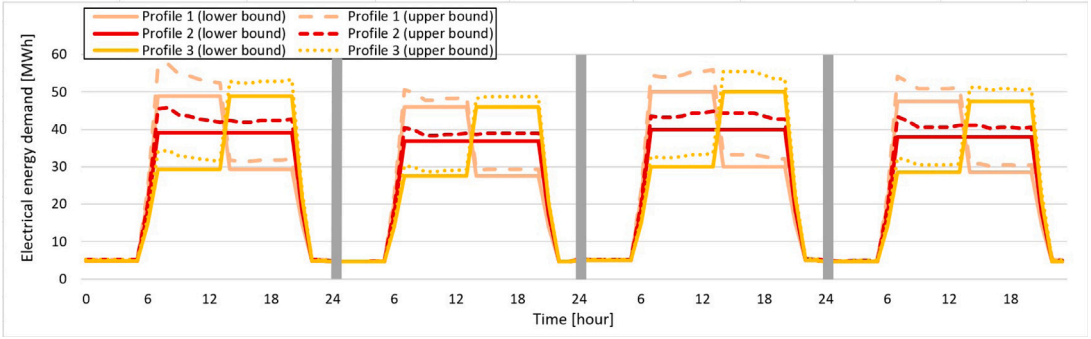

Fig. 5. The forecast bounds of industrial FD.

technologies, as reported in [46]. The specifications of the Li-ion ES are taken from [36] and provided in Table 3, while the details of the TPP are sourced from [35] and summarized in Table 4. The electrical energy consumption of the industrial FD is depicted in Fig. 5, based on three distinct consumption profiles derived from the hourly data in [38]. A flexibility margin of 10% is assumed for each base profile. The carbon emission factor of industrial FD is 0.4 tons CO_2/MW. The CO_2 emission quotas for TPP and industrial FD, based on their maximum generation and consumption levels, are 10 and 15 tons CO_2/MW, respectively. The carbon emission data for the TPP and industrial FD are estimated based on information from [34]. The forecast bounds for electricity prices in the DAM and SRM, along with the CTM price, are extracted from historical data reported in [47,48] and illustrated in Fig. 6. The main parameters used in the model are summarized in Table 5.

It is worth noting that each sample day corresponds to a different season and reflects the expected operating conditions during its respective time periods. For example, as shown in Fig. 4, the second and third sample days are characterized by high availability in PV and CSP output, which are typical of spring and summer. Conversely, the first and fourth sample days show lower production and greater variability, representative of winter and autumn conditions. Similarly, as seen in Fig. 5, the FD profiles also follow seasonal patterns, with higher consumption and greater fluctuations occurring on the first and third sample days.

Table 6 outlines the assumed uncertainty budgets assigned to various uncertain parameters across the case studies. Given that the solar PV production and the thermal power input of the SF in CSP are inactive during nighttime hours, they are allocated lower uncertainty budgets. This approach ensures a uniform proportion of hours with deviations across the entire simulation period for all uncertain parameters. It is important to note that the uncertainties are defined over two different temporal scopes. The DAM price, SRM price, RES production, CSP thermal production, and FD are modeled on an hourly basis for each season. In contrast, the CTM price is defined on whole seasons.

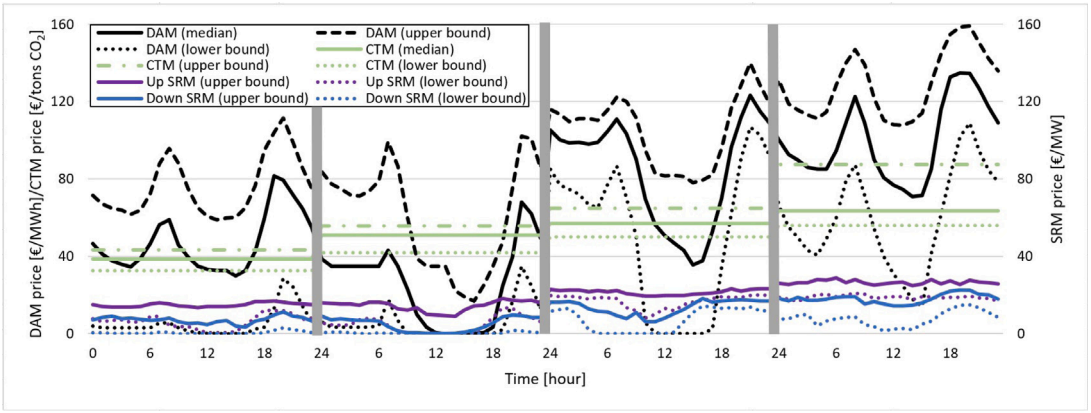

Fig. 6. The DAM, SRM, and CTM price data.

Table 2
CSP data.

SF/Turbine	Value	Molten salt TS	Value
SF maximum thermal power output [MW]	300	Maximum thermal energy [MWh]	1100
Turbine maximum thermal power input [MW]	140	Minimum thermal energy [MWh]	110
Turbine maximum electrical power output [MW]	55	Dis/charging thermal power [MW]	115/140
Turbine minimum up/down time [hour]	3/2	Dis/charging efficiency [%]	95

Table 3
Li-ion ES data.

Parameter	Value
Dis/charging power [MW]	15/15
Maximum/minimum energy [MWh]	50/5
Installation and expected operational costs [M€]	15
Degradation coefficient [–]	10^{-4}
Dis/charging efficiency [%]	95

Table 4
TPP data.

Parameter	Value
Maximum/minimum power output [MW]	50/20
Startup/shutdown cost [€]	500/200
Operation cost [€/MWh]	60
Minimum up/down time [hour]	3/1
Emission factor [tons CO_2/MW]	0.2

Table 5
Summary of main parameters used in the model.

Parameter	PV	WF	CSP	TPP	ES	FD	VPP
P_u [MW]	50	50	55	50	15	80	–
E_u [MWh]	–	–	–	–	50	500	–
C_u [€/MWh]	10	15	25	60	30	–	–
R_u^{SR} [MW/min]	2	2	10	10	15	5	–
η_u [%]	–	–	95	–	95	–	–
κ [%]	–	–	–	–	–	–	20
α_u [tons CO_2/MW]	–	–	–	0.2	–	0.4	–
ι_u [tons CO_2/MW]	–	–	–	10	–	15	–
T^{SR} [min]	–	–	–	–	–	–	15

Three case studies are performed to evaluate the effectiveness of the proposed model. The first case study (Case 1) focuses on the scheduling of VPP units, their carbon emissions, and the traded electrical energy and carbon credits in the deterministic strategy. It also examines how carbon credits are allocated across all sample days in the proposed model. The second case study (Case 2) investigates the ability of the proposed RO approach to manage various uncertainties. These include the DAM price, SRM price, CTM price, RES production, thermal output of CSP, and FD consumption. This case also analyzes the traded energy, reserve, and carbon credits under three different VPP operator strategies: optimistic, balanced, and pessimistic. Moreover, a sensitivity analysis is provided to examine the total profit of the VPP and carbon emissions from VPP units under different combinations and values of uncertainty budgets. In the third case study (Case 3), the traded carbon credits of the proposed model are compared with those from the model in [21] across varying levels of allowed carbon credits. Furthermore, the profitability and carbon emissions of the VPP using the proposed approach is assessed to highlight the benefits of the intertemporal approach over the daily approach. It is worth noting that the reason for selecting Ref. [21] as the benchmark is that several other studies, including [3,18,22,30,31], employ a similar carbon trading mechanism but are limited to a single sample day. While [21] also adopts the same carbon trading constraints, it extends the modeling framework to multiple sample days, which is more consistent with the multiple–sample-day structure used in this paper.

All simulations are conducted on a Dell XPS laptop equipped with an Intel i7-1165G7 2.8 GHz processor and 16 GB of RAM, using the CPLEX solver within the GAMS 49 environment. The proposed model is formulated as an MILP problem and is solved using the branch-and-cut algorithm employed by CPLEX. Across all tested case studies, the maximum computation time remains below five minutes, demonstrating the computational efficiency and tractability of the proposed RO approach for multi-market operation while accounting for intertemporal interactions. Further analysis of the model's computational performance, including the evolution of solution time and optimality gap under different VPP operator strategies, is provided in Section 4.2.

4.1. Case 1

Fig. 7 presents the traded electrical energy and reserve of the VPP in the DAM and SRM. It also shows the cumulative electrical energy output of the VPP units for the deterministic Case 1 across different sample days. The figure shows that on the first sample day, during hours 7–10, the VPP purchases energy in the DAM to supply its morning demand. This is because the output from the solar PV and CSP units is low during this period. At hour 9, the ES discharges to reduce the need for purchasing energy when electricity prices peak during the morning load hours. The CSP begins generating electricity at hour 11, and from that point onward, the VPP primarily becomes a net energy seller due to the increased availability of its generating units. On this sample day, Profile 1 in Fig. 5 is selected for the FD. As a result, the VPP can sell a

Table 6
Uncertainty budgets corresponding to different VPP strategies: optimistic, balanced, and pessimistic.

Strategy	DAM/SRM price	CTM price	WF production	PV production	CSP thermal production	FD consumption
Optimistic	4	1	4	3	3	4
Balanced	8	2	8	6	6	8
Pessimistic	12	3	12	9	9	12

larger amount of energy between hours 20–22, when electricity prices are higher (see Fig. 6). Additionally, at hour 20, the TPP starts up and begins producing energy, enabling the VPP to leverage the elevated electricity prices during hours 20–22. During hours 20–23, the CSP continues to generate energy. The ES also discharges at hour 20, further increasing the VPP's profit during the high-price hours.

On the second sample day, the VPP purchases energy in more hours compared to the first sample day, as the electricity price is very low during certain periods. Profile 3 of FD, shown in Fig. 5, is selected for this sample day. This profile features higher demand in the late hours, which aligns with the low electricity prices observed between hours 11–19 (see Fig. 6). During these hours, the VPP does not provide down reserve in the market, as most of its renewable production is curtailed. The VPP primarily sells energy during hours 8–11 and 22–24, when electricity prices are high, using various technologies such as WF, solar PV, CSP, and ES. During hours 22–24, the VPP provides more down reserve than up reserve. This is because most of its renewable units with production (WF and CSP) operate at maximum output, and the TPP is shut down in this sample day. In the third sample day, the TPP generates electricity for a greater number of hours—specifically, from hours 1–11 and 19–24. Additionally, RES such as solar PV and CSP exhibit high production after hour 9. Consequently, the VPP achieves a high production level and acts as an energy seller throughout the entire sample day. Moreover, due to the elevated generation levels across its units, the VPP provides more down reserve than up reserve. On the fourth sample day, the available energy from solar PV and CSP is lower compared to the second and third sample days. Therefore, the VPP operates the TPP throughout all time periods to take advantage of the high electricity prices observed on this sample day. Furthermore, as all VPP units are in operation, the VPP has sufficient capacity to offer both up and down reserves in most time periods.

Fig. 8 illustrates the contribution of each technology to the reserve provision, offering a more detailed insight into the VPP's reserve provision strategy. The figure shows that on the first and second sample days, the TPP either does not produce energy or operates for only a few hours (e.g., hours 20–22 on the first sample day). As a result, the main up reserve providers are the CSP and ES units, which can store energy for later use in case reserve requirements arise. The FD also contributes to the up reserve during some hours, although at a lower level compared to the CSP and ES. On both the first and second sample days, the amount of down reserve provided is lower than that of up reserve during most of the hours. The down reserve during these sample days is mainly supplied by the WF and solar PV units. However, during specific hours (hours 20–23 on the first sample day and hours 21–24 on the second sample day), the TPP and CSP also contribute to down reserve provision. This is due to their high production levels and their availability to reduce output if needed. Additionally, the ES contributes to down reserve in a few hours (hours 2, 3, and 20 on the first sample day, and hours 1 and 22 on the second sample day) to enhance the profitability of the VPP. On the third sample day, since the VPP units operate close to their maximum capacity, the up reserve provided is relatively low and is mainly covered by the ES and FD. However, most of the VPP units contribute to down reserve provision. On the last sample day, in addition to CSP, ES, and FD, the TPP plays a significant role in up reserve provision during some hours. A substantial amount of down reserve is also provided throughout this sample day, with the participation of most of the technologies.

Fig. 9 illustrates the carbon emissions of the TPP and the industrial FD. It also shows the traded carbon credits and the carbon credit allowances across different sample days in deterministic Case 1. In the proposed model, the VPP's allowable carbon emissions are adjusted daily based on its actual emission levels. Accordingly, the sum of the VPP's total emissions across all sample days and the traded carbon credits must remain below the total carbon allowance. Under the proposed approach, the VPP is only permitted to sell the surplus between its carbon credit allowance and actual emissions in the CTM. This restriction prevents profit generation through price arbitrage across different sample days. However, if the VPP emits more than its carbon allowance, it must purchase the excess credits from the market. The figure shows that carbon emissions from the TPP are kept minimal or zero in the first and second sample days, respectively. The higher TPP output on the third and last sample days leads to increased emissions aimed at enhancing VPP profitability. The industrial FD records its lowest emissions on the second sample day and its highest on the third. Notably, the VPP chooses to sell excess carbon credits on the last sample day, when the CTM price is higher compared to the other sample days (see Fig. 6).

4.2. Case 2

Fig. 10 presents the traded electrical energy of the VPP under different uncertainty-handling strategies in Case 2. Under the deterministic strategy, the VPP bids the highest amount of energy for sale in the DAM. It also bids the lowest amount for purchase during most hours, compared to the optimistic, balanced, and pessimistic strategies. In the optimistic strategy, the traded energy substantially differs from the deterministic case, but only during a few hours. For instance, on the first sample day between hours 16–23, the amount of energy sold decreases compared to the deterministic strategy. On the second sample day, hours 8, 19, and 21–23 show the most notable changes in traded energy. These hours typically correspond to high electricity prices (see Fig. 6), where uncertainty can significantly influence the VPP's profitability. On the third sample day, the traded energy is most affected during hours 6 and 10–14. As shown in Fig. 6, significant negative DAM price deviations during hours 10–14 compel the VPP to reduce its market participation. Conversely, during hour 6, the VPP increases its traded energy, suggesting a preference for operating in hours with lower uncertainty. A similar trend is observed on the last sample day. The optimistic strategy results in a substantial reduction of traded energy during hours 11–14, 18, and 19, while only a few hours – such as hour 22 – exhibit increased trading activity compared to the deterministic case. In the balanced and pessimistic strategies, a greater number of hours are selected as worst-case periods. Consequently, more significant changes in the traded energy of the VPP occur compared to the deterministic and optimistic strategies. In some instances, even the direction of traded energy is reversed. For example, on the first sample day under the pessimistic strategy, the VPP purchases energy in the DAM during hours 11–13 and 15–18, whereas it was a seller in the deterministic case. On the last two sample days, however, the VPP remains an energy seller in all hours, even under the pessimistic strategy. This is because all VPP units are available for energy production during these sample days, allowing different units to compensate for each other's energy shortfalls.

Fig. 11 shows the traded up and down reserves while considering different uncertainty-handling strategies in Case 2. A reduction in energy production by VPP units can create additional capacity for up

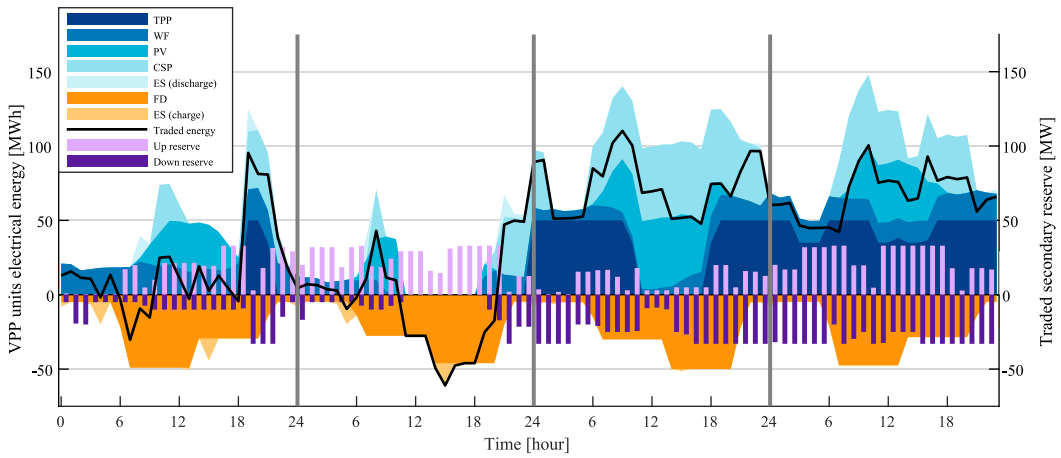

Fig. 7. The VPP units electrical energy and the VPP traded electrical energy and reserve in Case 1.

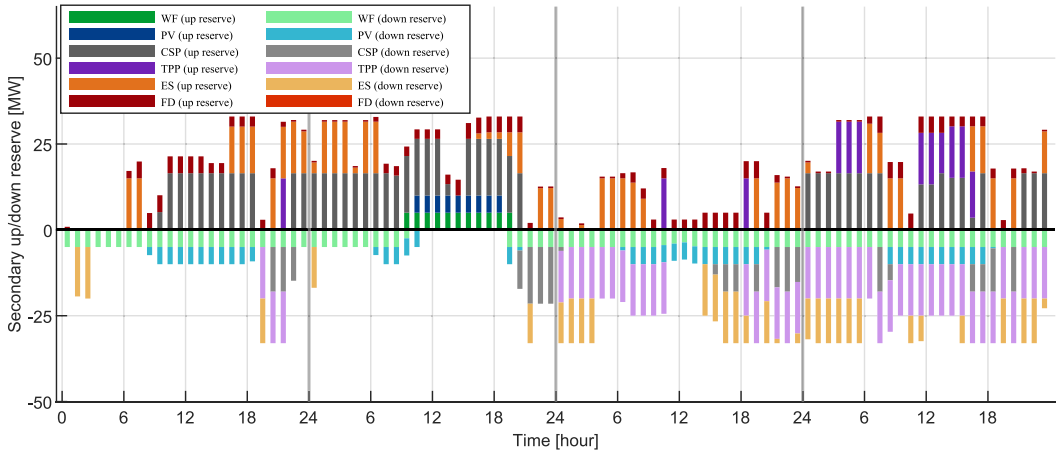

Fig. 8. The VPP units provided up and down reserve in Case 1.

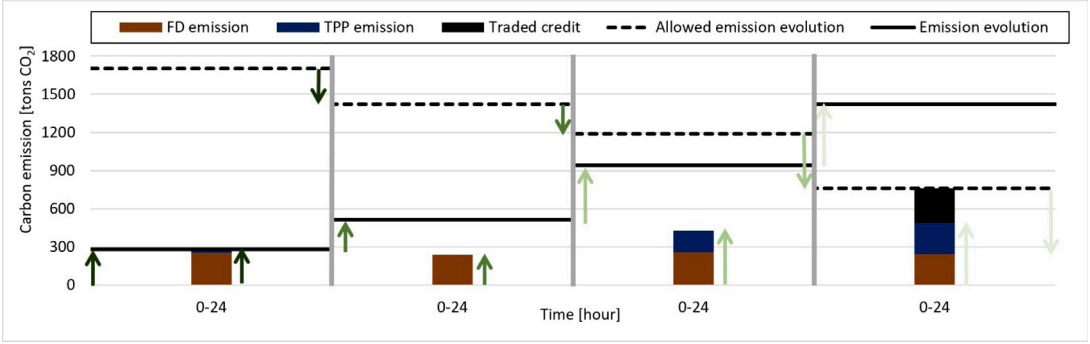

Fig. 9. Carbon emission of different VPP units and traded carbon credits in Case 1.

reserve provision while simultaneously lowering the available capacity for down reserve. For example, on the first sample day between hours 1–4, the up reserve provided by the VPP under the balanced and pessimistic strategies increases compared to the deterministic strategy. Similarly, the down reserve during hours 2–3 is reduced across all non-deterministic strategies (optimistic, balanced, and pessimistic) compared to the deterministic strategy. This is because the reserve provision by the VPP is influenced not only by SRM price uncertainty but also by other factors, such as the energy traded in the DAM. Specifically, during hours 1–4 in the balanced and pessimistic strategies, the traded energy is reduced compared to the deterministic strategy. This reduction leads to increased up reserve and decreased down reserve. This mutual interaction between energy and reserve provision under uncertainty is also observed during hours 12–18 on the third sample day. In this period, energy provision in the DAM decreases under uncertainty (see Fig. 10), while the up reserve increases and the down reserve decreases (see Fig. 11). However, there are also instances where uncertainty negatively impacts the VPP's participation in both the DAM and SRM—including traded energy, up reserve, and down reserve. For example, during hours 12–18 on the last sample day, all these variables decrease across the optimistic, balanced, and pessimistic strategies compared to the deterministic strategy.

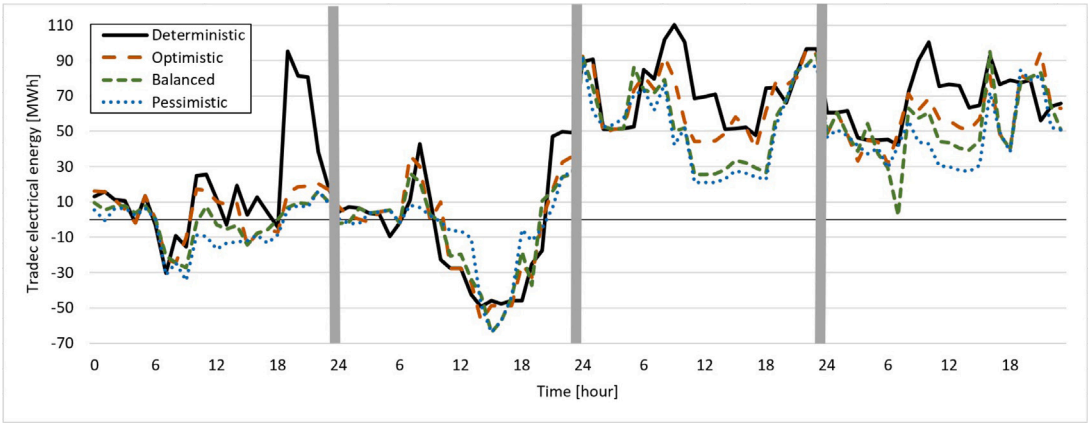

Fig. 10. Electrical energy traded by the VPP under different uncertainty-handling strategies in Case 2.

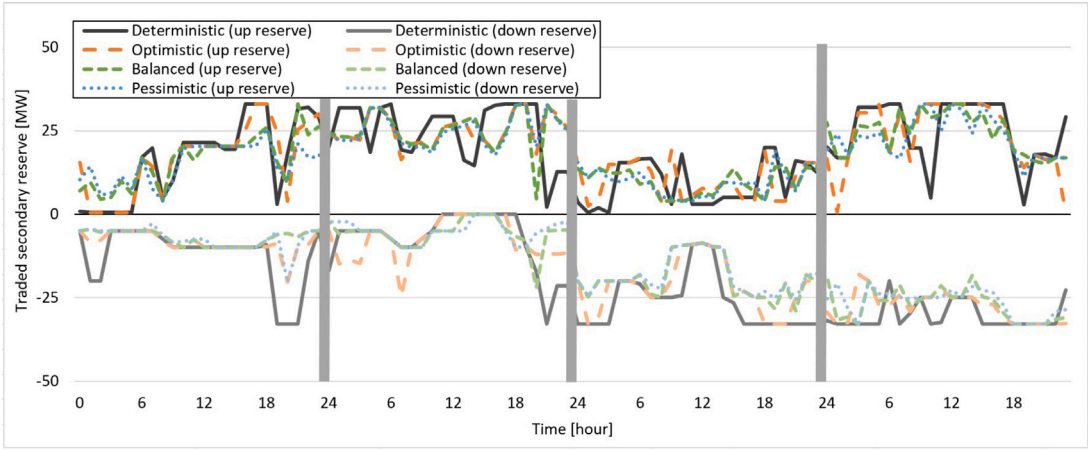

Fig. 11. Traded up and down reserves by the VPP under different uncertainty-handling strategies in Case 2.

Fig. 12 shows the carbon emissions of VPP units and the traded carbon credits as a function of the CTM price, under different uncertainty-handling strategies in Case 2. When uncertainty is considered, industrial demand consumption generally increases, leading to higher emissions. As a result, the industrial FD produces the highest emissions under the pessimistic strategy across all sample days. However, under more conservative strategies, the VPP tends to generate less energy through the TPP, resulting in reduced emissions from that unit. The reduced production of VPP units, particularly the TPP, is driven by uncertainty in DAM prices. This uncertainty lowers profitability and leads to a decrease in energy production. This figure also shows that, in some strategies, the VPP prefers to trade carbon credits on a sample day other than the last one. Although the CTM price is highest on the last sample day, the associated uncertainty may impact this price. Therefore, under the optimistic strategy, the VPP opts to sell part of its carbon credits on the third sample day to avoid potential price fluctuations on the last sample day.

Fig. 13 illustrates the computational performance of the proposed model, displaying the objective function value and optimality gap over time for various VPP operator strategies. The marked points on the graph indicate the solver's objective value and optimality gap at different iterations. The results show that the optimality gap decreases efficiently and that the objective function converges rapidly toward its final optimal value. For instance, in all strategies, the optimality gap falls below 0.01 p.u. within 20 s. These findings confirm the robustness and efficiency of the proposed model in reaching optimal solutions under different uncertainty-handling strategies.

Fig. 14 presents the sensitivity analysis of the total profit of the VPP for different combinations and values of uncertainty budgets in Case 2. These include uncertainties related to *energy* (i.e., solar PV and WF electrical production, CSP thermal production, and FD consumption), uncertainties related to *price* (i.e., DAM, SRM, and CTM prices), and a combined *price* & *energy* uncertainty case, which includes all sources of uncertainty. The uncertainty budgets for all uncertain parameters range from 0 to 24, except for the CTM price, which varies from 0 to 4. To present all cases on a consistent x-axis, the uncertainty budget is normalized and shown in per-unit (p.u.) terms, where 1 p.u. corresponds to the maximum possible budget (i.e., 24 for most uncertainties, and 4 for the CTM price). The figure shows that as the uncertainty budget increases, the VPP's profit decreases. This is because the VPP adopts more conservative bidding strategies in response to higher uncertainty. The decline is more pronounced when all uncertainties are considered, compared to cases with only price or only energy uncertainties. For instance, when all uncertainties are active, profit decreases by 37.8%, 59.3%, 71.6%, and 77.5% at uncertainty budgets of 0.25, 0.5, 0.75, and 1 p.u., respectively, relative to the deterministic case (0 p.u.). In comparison, when only price-related uncertainties are considered, the profit reductions are 21.1%, 32.4%, 40.4%, and 44.7%, while for energy-related uncertainties, the reductions are 19.4%, 31.9%, 38.6%, and 42.3%, respectively.

Fig. 15 shows the sensitivity analysis of carbon emissions from the VPP units in Case 2 for different uncertainty budgets, defined similarly to those in Fig. 14. The results indicate that as the uncertainty budget increases, carbon emissions from the TPP generally decrease under

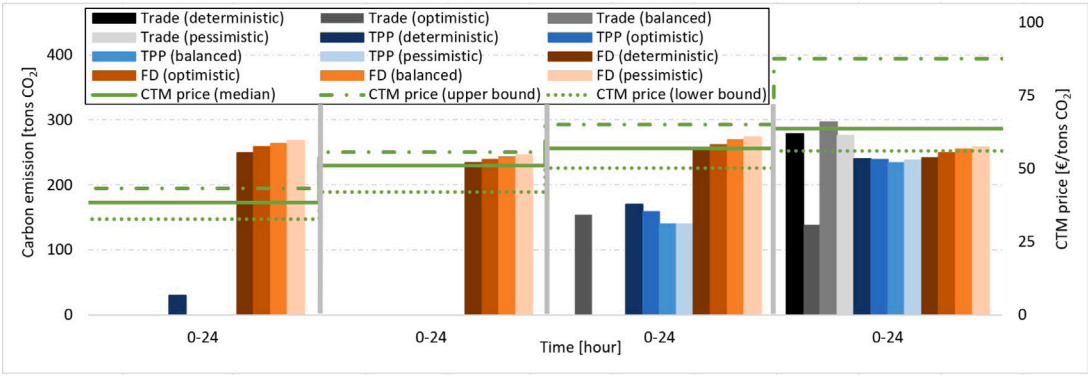

Fig. 12. Carbon emissions from VPP units and carbon credit trading under different uncertainty-handling strategies in Case 2.

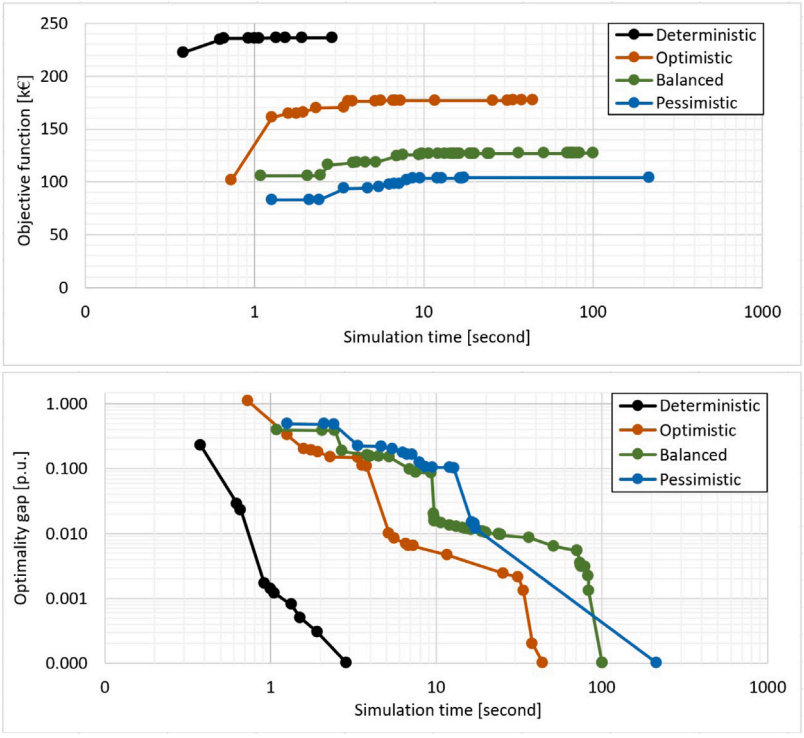

Fig. 13. Evolution of the objective function and optimality gap during the simulation in Case 2.

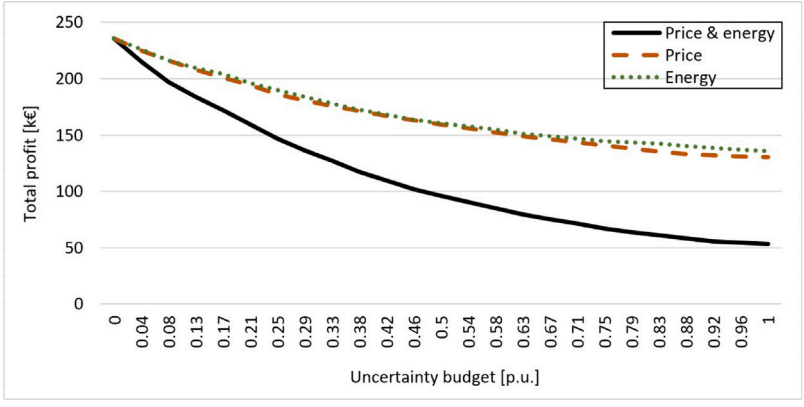

Fig. 14. VPP profit in Case 2 for different uncertainty budgets: **Price & energy:** $\left(\Gamma_r, \Gamma_\theta, \Gamma_d, \Gamma^{DA}, \Gamma^{SR,\uparrow}, \Gamma^{SR,\downarrow} \in [0,24],\ \Gamma^{CA} \in [0,4]\right)$; **Price:** $\left(\Gamma_r, \Gamma_\theta, \Gamma_d = 0,\ \Gamma^{DA}, \Gamma^{SR,\uparrow}, \Gamma^{SR,\downarrow} \in [0,24],\ \Gamma^{CA} \in [0,4]\right)$; **Energy:** $\left(\Gamma_r, \Gamma_\theta, \Gamma_d \in [0,24],\ \Gamma^{DA}, \Gamma^{SR,\uparrow}, \Gamma^{SR,\downarrow}, \Gamma^{CA} = 0\right)$.

two uncertainty combinations: price, and price & energy. This occurs because the VPP adopts a more conservative market strategy under higher uncertainty, leading to reduced energy sales and, consequently, lower production and emissions from the TPP. In contrast, when only energy-related uncertainties are considered, emissions from the TPP remain mostly constant across the uncertainty budget range. This suggests that, to compensate for energy shortfalls from RES, the VPP prefers to reduce its market sales rather than increase the output of the TPP. However, a smaller reduction in emissions is observed when both price and energy uncertainties are considered compared to the case with only price uncertainties. This suggests that the VPP is less inclined to further reduce TPP output to cover energy shortages from the RES. Therefore, the extent of TPP production reduction depends on the specific combination of uncertainties considered.

The results for FD in Fig. 15 emissions show that they are primarily influenced by energy uncertainties. As the energy uncertainty budget increases, the FD's energy consumption – and therefore its emissions – also increase. Conversely, when only price uncertainties are considered, the VPP tends to keep FD consumption low across all uncertainty levels to minimize emissions. Total emissions, defined as the sum of emissions from the TPP and FD, can either increase or decrease with a rising uncertainty budget, depending on which uncertainties are considered. When only energy uncertainties are accounted for, total emissions increase with the uncertainty budget, mainly due to the growing FD emissions. When only price uncertainties are included, total emissions tend to decrease, driven by reduced TPP output and stable FD consumption. Finally, when both price and energy uncertainties are considered, total emissions initially rise – due to the dominant effect of increasing FD emissions – but eventually decline as FD emissions saturate, while the decreasing TPP emissions become more dominant.

4.3. Case 3

Fig. 16 compares the VPP's traded carbon credits under varying carbon credit allowances (0%–100% relative to Cases 1 and 2), using both the proposed model and the model in [21], in Case 3. These varying allowances represent future outlooks with higher RES integration and, consequently, reduced free carbon allocations for polluting units. In [21], carbon credit trading is modeled for four sample days without considering their interactions. Therefore, for comparison purposes, credit transactions are assumed to be independent for each sample day in the simulations of the model in [21]. In contrast, the proposed model requires that the cumulative carbon credit balance be satisfied only by the end of the last sample day. This approach provides the VPP with greater flexibility to optimize carbon credit trading when CTM prices are more favorable. Under a 100% carbon allowance in the proposed model, the VPP sells its surplus carbon credits on the last sample day, when the CTM price is highest. In contrast, in [21], the VPP has excess credits during the first and second sample days and sells these credits on the corresponding sample days. On the third and last sample days, the VPP emits more carbon and thus has little to no surplus credit to sell in the CTM. In particular, during the last sample day, the emissions from the VPP exceed the allowed carbon credits, requiring the purchase of additional credits. As the allowed carbon credit decreases from 100% to 0%, the VPP increasingly relies on purchasing carbon credits from the market. In the proposed model, the VPP strategically chooses to purchase its required carbon credits on the first sample day, when the CTM price is relatively low. However, in [21], credit purchases are made independently on each sample day without considering prices across the time horizon. For instance, under the 25% carbon allowance, the VPP in [21] purchases the highest amount of carbon credits during the last period—when both emissions and CTM prices are highest. Therefore, the strategy in [21] overlooks a key advantage: the ability of the VPP to offset high-emission sample days by acquiring credits on lower-cost sample days. The proposed model captures this intertemporal flexibility, enabling more cost-effective carbon credit management.

Table 7 compares the carbon emissions from VPP units under the proposed approach, the model in [21], and a baseline case in which neither CTM nor carbon constraints are considered. Comparing the proposed approach with the case where CTM is not considered, carbon emissions from the FD are reduced by 15.8%, 12.1%, 9.9%, and 7.9% under the deterministic, optimistic, balanced, and pessimistic uncertainty-handling strategies, respectively. For the TPP, the corresponding reductions are 20.3%, 6.0%, 10.8%, and 15.1%. The total carbon emissions of all units are reduced by 17.3%, 10.5%, 10.2%, and 10.0% under the same strategies. These results highlight the importance of including carbon emission constraints to support carbon neutrality goals. Compared to the model in [21], the proposed approach achieves equal or lower carbon emissions. To better understand the effect of intertemporal carbon trading on emission reduction, the absolute differences in carbon emissions between each approach and the baseline without considering CTM are compared. For the TPP, the emission reductions in the model in [21] are 102, 25.5, 32.4, and 58.8 tons of CO_2 for the deterministic, optimistic, balanced, and pessimistic strategies, respectively. In comparison, the proposed approach yields reductions of 112, 25.5, 45.4, and 67.3 tons of CO_2, which are 9.8%, 0%, 40.1%, and 14.5% higher than those achieved by the model in [21]. For the total emissions of all units, the corresponding improvements are 3.5%, 0%, 8.9%, and 5.7%. The superior performance of the proposed approach is attributed to its ability to account for intertemporal carbon credit trading. Unlike the model in [21], which considers the carbon price only on each individual sample day and may allow high-emission operation when CTM prices are low, the proposed model enables the VPP to optimize across multiple sample days, storing credits when prices are low and trading them when prices are high. This flexibility enables more effective trading and leads to lower overall emissions.

Table 8 compares the VPP's total profit and the profit or cost of trading in the CTM (with negative values indicating cost) in Case 3. The results show that the proposed approach improves the VPP's total profitability compared to the model in [21]. For 100%, 75%, 50%, 25%, and 0% allowed carbon credits, the increases are 5.8%, 9.2%, 22.6%, 51.0%, and 150.7%, respectively. Additionally, the proposed model achieves a greater profit increase or cost reduction in the CTM compared to the model in [21], with improvements of 55.3%, 44.5%, 32.4%, 29.9%, and 29.0%, respectively, for the same carbon credit allowances. The 29–55.3% increase in CTM profit in the proposed model is achieved by allowing carbon credit trading across multiple sample days rather than limiting it to daily trading. Unlike the model in [21], which restricts trading decisions to the same sample day the emissions are generated, the proposed approach adopts a more flexible intertemporal decision-making framework. This enables the VPP to offset emissions from high-pollution sample days by purchasing credits on sample days with lower carbon costs, or to sell excess credits on sample days with higher CTM prices. These results highlight the importance of the proposed model in enhancing the VPP's profitability by adopting an optimized strategy across all sample days for participation in the CTM.

Fig. 17 presents various financial metrics of the VPP for different levels of allowed carbon credit in Case 3. The revenue sources include energy trading in the DAM, reserve trading in the SRM, and carbon credit trading in the CTM. If the VPP purchases carbon credits from the CTM, this appears as a negative value in the figure, representing a cost. The figure also shows the operational costs of the VPP units and the robust cost. The robust cost reflects the negative impact of deviations in the DAM, SRM, and CTM prices on the objective function (13a), as defined in Section 3.2.3. The total profit of the VPP is calculated as the sum of all revenues minus the operational and robust costs. The figure shows that, across all levels of allowed carbon credit, most of the VPP's revenue comes from energy trading in the DAM. The results also demonstrate that, under the proposed approach – which accounts

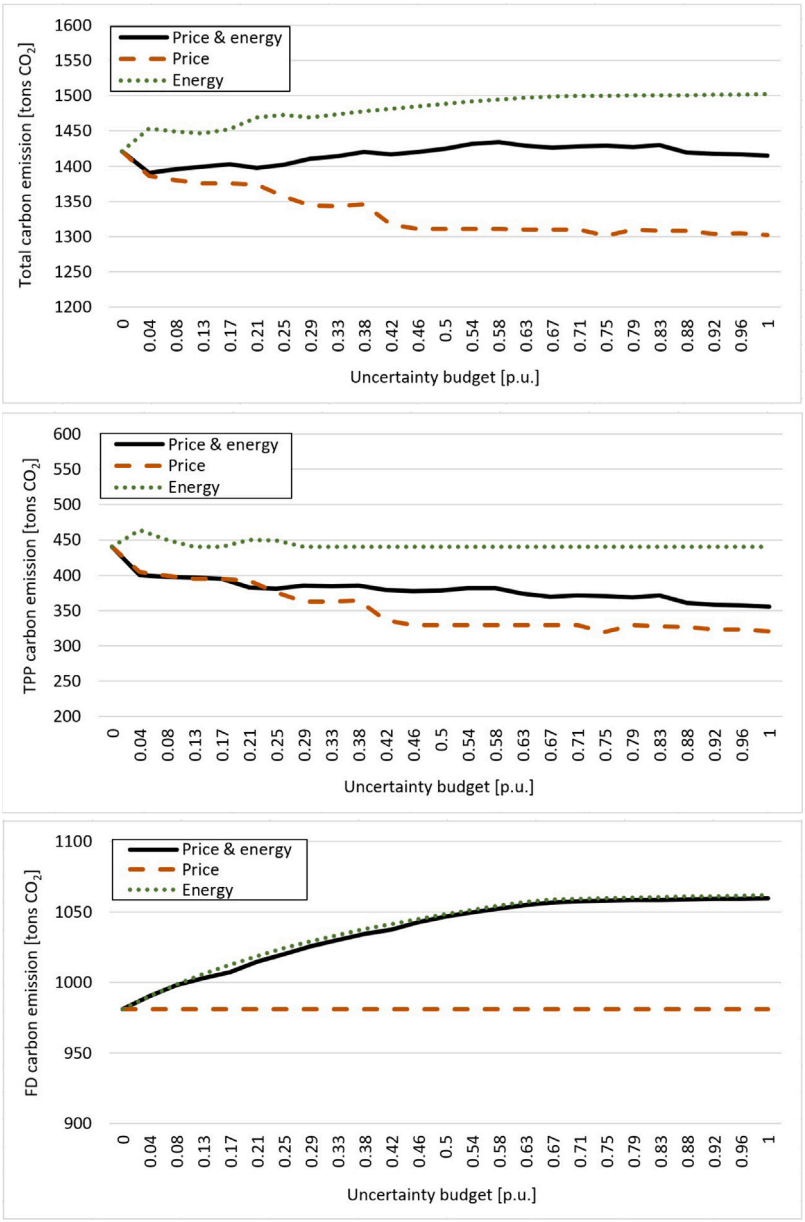

Fig. 15. Carbon emissions from VPP units in Case 2 for different uncertainty budgets: **Price & energy:** $\left(\Gamma_r, \Gamma_\theta, \Gamma_d, \Gamma^{DA}, \Gamma^{SR,\uparrow}, \Gamma^{SR,\downarrow} \in [0,24],\ \Gamma^{CA} \in [0,4]\right)$; **Price:** $\left(\Gamma_r, \Gamma_\theta, \Gamma_d = 0,\ \Gamma^{DA}, \Gamma^{SR,\uparrow}, \Gamma^{SR,\downarrow} \in [0,24],\ \Gamma^{CA} \in [0,4]\right)$; **Energy:** $\left(\Gamma_r, \Gamma_\theta, \Gamma_d \in [0,24],\ \Gamma^{DA}, \Gamma^{SR,\uparrow}, \Gamma^{SR,\downarrow}, \Gamma^{CA} = 0\right)$.

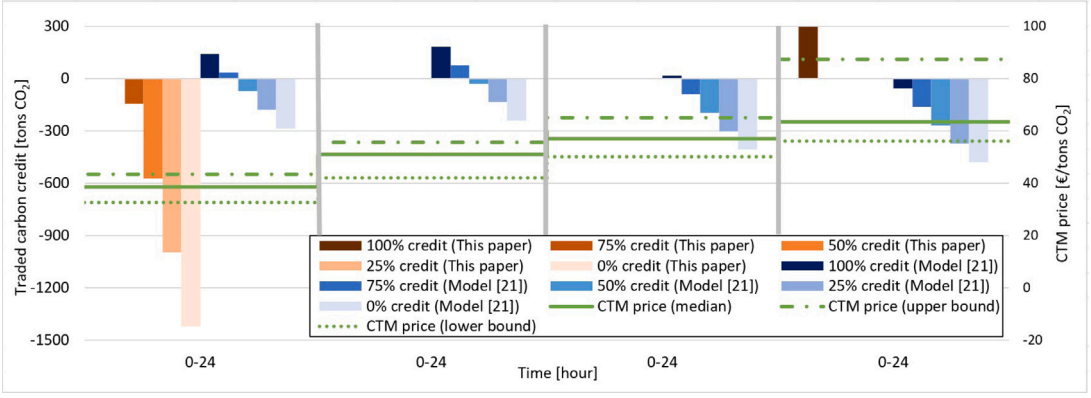

Fig. 16. The VPP carbon credit trading by considering different allowed carbon credit level in Case 3.

Table 7
Carbon emissions of VPP units for the proposed model and the model in [21] in Case 3.

Strategy	FD carbon emission [tons CO_2]			TPP carbon emission [tons CO_2]			Total carbon emission [tons CO_2]		
	W/o CTM	This paper	Model [21]	W/o CTM	This paper	Model [21]	W/o CTM	This paper	Model [21]
Deterministic	1165.8	981.0	981.0	552.0	440.0	450.0	1717.8	1421.0	1431.0
Optimistic	1148.2	1008.9	1008.9	423.3	397.8	397.8	1571.5	1406.7	1406.7
Balanced	1143.8	1030.2	1030.2	419.3	373.9	386.9	1563.2	1404.1	1417.1
Pessimistic	1137.0	1046.6	1046.6	445.1	377.8	386.3	1582.2	1424.3	1432.8

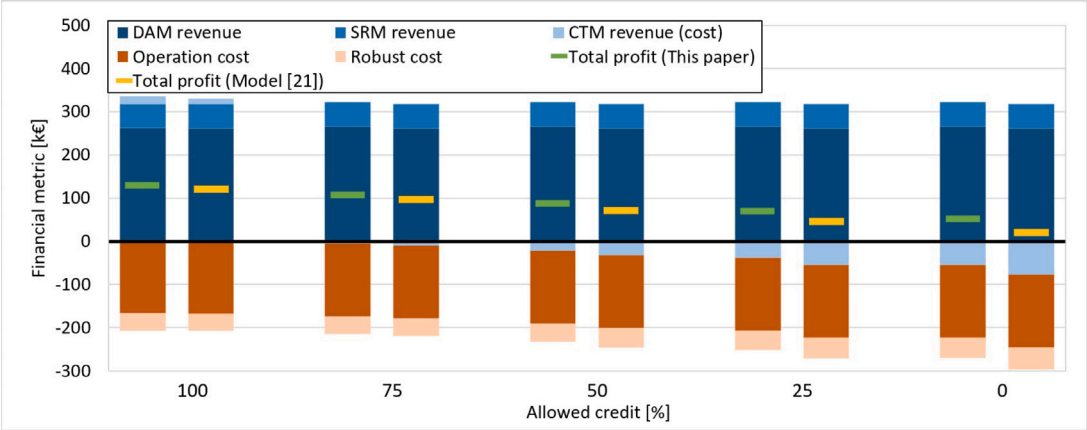

Fig. 17. The VPP financial metrics by considering different allowed carbon credit level in Case 3.

Table 8
The VPP total profit and CTM profit for the proposed model and the model in [21] in Case 3.

Allowed credit [%]	Total profit [k€]		CTM profit (cost) [k€]	
	This paper	Model [21]	This paper	Model [21]
100	128.7	121.6	18.8	12.1
75	106.6	97.6	−5.6	−10.1
50	88.2	71.9	−21.9	−32.4
25	69.8	46.2	−38.3	−54.7
0	51.4	20.5	−54.7	−77.1

for intertemporal carbon trading – the revenue from carbon credit sales by the VPP when it acts as a seller (e.g., at 100% allowed credit) is higher than in [21]. Conversely, when the VPP purchases carbon credits (e.g., for 0%–75% allowed credit), its costs are lower than in [21]. As a result, the proposed model achieves a higher total profit across all levels of allowed carbon credit compared to the approach in [21].

4.4. Future work, validation, and practical considerations

Future work will focus on validating and extending the proposed model using additional real-world operational data from existing VPPs or regional energy systems, ensuring compliance with current ETS regulations and practical aggregator capabilities. For instance, historical market prices, carbon allowance trading records, and unit-level generation and emissions data – similar to those already used in this study – could be leveraged to calibrate and test model performance under diverse operating conditions.

To align with ETS policies, the model's intertemporal carbon credit trading logic could be adapted to reflect jurisdiction-specific rules on banking, borrowing, or credit expiration. Aggregator-specific limitations, such as transaction caps, minimum bid sizes, or participation thresholds, could be incorporated as additional operational constraints. These enhancements would help ensure that the model's recommendations remain feasible in real market settings.

From a methodological perspective, advanced stochastic modeling approaches could be explored to capture intertemporal CTM price volatility while preserving computational tractability. Incorporating such methods would allow the model to account for a wider range of possible price trajectories, quantify probabilistic risk measures, and improve decision-making under uncertainty. Future work could also extend this framework by incorporating a larger set of sample days to more accurately approximate real-time operational dynamics. Collaborations with industry stakeholders or access to open datasets from system operators (e.g., ENTSO-E, EU ETS registries) could further improve practical relevance and credibility. Finally, implementing the model in a live pilot setting would provide valuable insights into operational feasibility, cost–emissions trade-offs, and decision-support value for VPP operators under actual market and policy conditions.

5. Conclusion

In this paper, a novel two-stage robust model is proposed for the DAM and SRM participation of VPP, as well as for trading carbon credits in the CTM. The VPP in this model includes both renewable units – such as a wind farm, solar PV plant, and CSP equipped with thermal storage – and electrical storage, as well as polluting units, such as a TPP and industrial flexible demand. Unlike existing models in the literature, the proposed model incorporates carbon credit trading over four sample days, accounting for their interactions. This allows the VPP to offset its emissions on a particular sample day by trading on other sample days and to leverage differences in CTM prices across sample days to sell extra carbon credits. Multiple uncertainties related to DAM, SRM, and CTM prices, as well as renewable energy production and demand consumption, are incorporated into the optimization problem. Three case studies are conducted to demonstrate the applicability of the proposed approach, exploring different countermeasure strategies against uncertain parameters and investigating the effects of varying carbon credit allowances for the polluting units of the VPP.

The simulation results show that the VPP schedules its units across different sample days based on their available energy to maximize profitability by trading various commodities in the markets. Specifically, on sample days when the predicted electricity price is low, the VPP either does not operate the TPP unit or operates it for only a few hours to minimize carbon emissions. However, on sample days

when electricity prices are high or renewable energy production is insufficient, the VPP takes advantage of the TPP to increase profitability in the market. The results also show that CSP and electrical storage contribute significantly to providing up reserve in the SRM, owing to their ability to store energy. The down reserve is provided by most of the VPP units, depending on their availability. Furthermore, adopting more conservative strategies in response to uncertain parameters leads the VPP to sell less electricity when acting as a seller and to purchase more when acting as a buyer in the DAM. The up and down reserves provided by the VPP can be mutually affected by the traded energy in the DAM. Specifically, when the sold energy of the VPP decreases in the DAM due to uncertainty, up and down reserves can increase and decrease, respectively, due to more or less capacity for providing each reserve from the VPP in the market. The simulation also shows that, with the proposed approach, the VPP leverages CTM price differences between sample days by trading its extra or required carbon credits on sample days with more favorable prices. This leads to an increase in total profitability and CTM profitability by 5.8–150.7% and 29.0–55.3%, respectively, compared to models in the literature where the interactions between different sample days are neglected.

CRediT authorship contribution statement

Hadi Nemati: Writing – review & editing, Writing – original draft, Visualization, Validation, Software, Methodology, Investigation, Formal analysis, Data curation, Conceptualization. **Álvaro Ortega:** Writing – review & editing, Validation, Supervision, Resources, Project administration. **Pedro Sánchez-Martín:** Writing – review & editing, Validation, Supervision.

Declaration of competing interest

The authors declare that they have no known competing financial interests or personal relationships that could have appeared to influence the work reported in this paper.

Acknowledgments

The authors wish to thank Comunidad de Madrid for the financial support to PREDFLEX project (TEC-2024/ECO-287), through the R&D activity programme Tecnologías 2024.

Appendix A. Detailed nomenclature

This appendix contains the complete nomenclature, offering comprehensive definitions of all variables and parameters employed in the study.

Detailed Nomenclature

Indexes and Sets

$c \in \mathcal{C}$	Set of TPPs
$d \in \mathcal{D}$	Set of FDs
$m \in \mathcal{M}$	Set of daily load profiles
$r \in \mathcal{R}$	Set of RES
$s \in \mathcal{S}$	Set of ESs
$t \in \mathcal{T}$	Set of time periods in each sample day
$t \in \mathcal{T}^{CT}$	Set of sample days in which the worst case of CTM price uncertainty occurs
$t \in \mathcal{T}^{DA/SR}$	Set of time periods in which the worst case of DAM/SRM price uncertainty occurs
$t \in \mathcal{T}^{Day}$	Set of sample days
$t \in \mathcal{T}_{\theta}$	Set of time periods in which the worst case of CSP θ thermal production uncertainty occurs
$t \in \mathcal{T}_{d}$	Set of time periods in which the worst case of FD d consumption uncertainty occurs
$t \in \mathcal{T}_{r}$	Set of time periods in which the worst case of RES r electrical production uncertainty occurs
$\theta \in \Theta$	Set of CSPs
$\Xi^{DA+SR+CT}$	Set of decision variables of DAM, SRM, and CTM

Parameters

C_c^{SD}	Shut-down costs of TPP c	[€]
C_c^{SU}	Start-up costs of TPP c	[€]
C_c	Operation and maintenance costs of TPP c	[€/MWh]
$C_{r(\theta)}$	Operation and maintenance costs of RES r (CSP θ)	[€/MWh]
C_s	Installation and expected operational costs of ES s	[€]
E_d	Electrical energy consumption of FD d throughout the time horizon	[MWh]
E_s	Electrical energy capacity of ES s	[MWh]
K_{θ}	Start up electrical output multiplier of turbine of CSP	[p.u.]
M	Big positive value	[–]
M_s	Coefficient of degradation of ES s	[–]
$N_c^{OFF/ON}$	Number of initial periods during which TPP c must be offline/online	[h]
P_d	Electrical power consumption of FD d	[MW]
$P_{\theta,t}^{SF}$	Thermal power production forecast of SF of CSP θ during period t	[MW]
P_c	Electrical power production of TPP c	[MW]
$P_{d,m,t}$	FD d profile m consumption forecast during period t	[MW]
$P_{r(\theta)}$	Electrical power production of RES r (CSP θ)	[MW]
$P_{r,t}$	RES r production forecast during period t	[MW]
P_s	Electrical power capacity of ES s	[MW]
R_c^{SR}	Secondary reserve ramp rate of TPP c	[MW/min]
R_d^{SR}	Secondary reserve ramp rate of FD d	[MW/min]
$R_{r(\theta)}^{SR}$	Secondary reserve ramp rate of RES r (CSP θ)	[MW/min]
T^{SR}	Required time for secondary reserve action	[min]
UT_c/DT_c	Minimum up/down time of turbine of TPP c	[h]
α_c	Emission factor of TPP c	[tons CO_2/MW]
α_d	Emission factor of FD d	[tons CO_2/MW]
$\beta_{d,t}$	Percentage of flexibility of FD d during period t	[%]
$\Gamma^{DA/SR/CT}$	Uncertainty budget of DAM/SRM/CTM price	[–]
Γ_d	Uncertainty budget of consumption of FD d	[–]
$\Gamma_{r(\theta)}$	Uncertainty budget of RES r electrical (SF of CSP θ thermal) production	[–]
Δt	Duration of periods	[h]
η_{θ}	Thermal to electrical output efficiency of CSP θ	[%]
η_s	Electrical power efficiency of ES s	[%]
ι_c	Emission quotas for TPP c	[tons CO_2/MW]

ι_d	Emission quotas for FD d	[tons CO_2/MW]
κ	Percentage of reserve traded in the SRM relative to the power capacity of VPP	[%]
λ_t^{CT}	CTM price during sample day t	[€/tons CO_2]
λ_t^{DA}	DAM price during period t	[€/MWh]
$\lambda_t^{SR,\uparrow(\downarrow)}$	SRM price for up (down) reserve during period t	[€/MW]

Variables

$e_{s,t}$	Electrical energy of ES of s during period t	[MWh]
$n^{Allocated}$	Free carbon credits allocated to VPP	[tons CO_2]
n_t^{Buy}	Carbon credits purchased by VPP during sample day t	[tons CO_2]
n_t^{CT}	Carbon credits traded by VPP during sample day t	[tons CO_2]
n_t^{Saved}	Carbon credits saved by VPP during sample day t for its emission	[tons CO_2]
n_t^{Sell}	Carbon credits sold by VPP during sample day t	[tons CO_2]
n_t^{Used}	Carbon credits used by VPP during sample day t from its freely allocated allowance	[tons CO_2]
n^{VPP}	Total carbon credits required by VPP	[tons CO_2]
$n_t^{Allowed}$	Allowed carbon emissions for VPP during sample day t	[tons CO_2]
$n_{c,t}$	Carbon credits required by TPP c during period or sample day t	[tons CO_2]
$n_{d,t}$	Carbon credits required by FD d during period or sample day t	[tons CO_2]
p_t^{DA}	Electrical power traded by VPP in the DAM during period t (positive/negative for selling/buying)	[MW]
$p_{\theta,t}^{SF}$	Thermal power of SF of CSP θ during period t	[MW]
$p_{\theta,t}^{TS}$	Thermal power of TS of CSP θ during period t	[MW]
$p_{c,t}$	Electrical production of TPP c during period t	[MW]
$p_{d,t}$	Electrical consumption of FD d during period t	[MW]
$p_{r(\theta),t}$	Electrical production of RES r (CSP θ) during period t	[MW]
$p_{s,t}$	Electrical power of ES s during period t	[MW]
r_t^{SR}	Reserve traded by VPP in the SRM during period t	[MW]
$r_{c,t}$	Reserve provided by TPP c during period t	[MW]
$r_{d,t}$	Reserve provided by FD d during period t	[MW]
$r_{r(\theta),t}$	Reserve provided by RES r (CSP θ) during period t	[MW]
$r_{s,t}$	Reserve provided by ES s during period t	[MW]
w_t^{CT}	Positive auxiliary variable of CTM price uncertainty during sample day t	[–]
$w_t^{DA/SR}$	Positive auxiliary variable of DAM/SRM price uncertainty during period t	[–]
$w_{d,t}$	Positive auxiliary variable of FD d consumption uncertainty during period t	[–]
$w_{r(\theta),t}$	Positive auxiliary variable of RES r electrical (SF of CSP θ thermal) production uncertainty during period t	[–]
z_t^{CT}	Positive auxiliary variable of traded carbon credits in the CTM during sample day t	[tons CO_2]
z_t^{DA}	Positive auxiliary variable of traded electrical energy in the DAM during period t	[MWh]
$z_{d,t}$	Positive auxiliary variable of FD d consumption uncertainty during period t	[MW]
$z_{r(\theta),t}$	Positive auxiliary variable of RES r electrical (SF of CSP θ thermal) production uncertainty during period t	[MW]
$\delta^{DA/SR/CT}$	Dual variable to model the DAM/SRM/CTM price uncertainty	[€]
δ_d	Dual variable to model the FD d consumption uncertainty	[MW]
$\delta_{r(\theta)}$	Dual variable to model the RES r electrical (SF of CSP θ thermal) production uncertainty	[MW]
σ_s	Share of energy capacity of ES s allocated to provide reserve	[%]
ψ_t^{CT}	Dual variable to model the CTM price uncertainty during sample day t	[€]
$\psi_t^{DA/SR}$	Dual variable to model the DAM/SRM price uncertainty during period t	[€]
$\psi_{d,t}$	Dual variable to model the FD d consumption uncertainty during period t	[MW]
$\psi_{r(\theta),t}$	Dual variable to model the RES r electrical (SF of CSP θ thermal) production uncertainty during period t	[MW]

Binary Variables

u^{CT}	Binary variable that is 1 if VPP is carbon credit seller, and 0 otherwise	[–]
$u_{c(\theta),t}$	Binary variable that is 1 if turbine of TPP c (CSP θ) is on during period t, and 0 otherwise	[–]
$u_{d,m}$	Binary variable that is 1 if profile m of demand d is selected, 0 otherwise	[–]
$u_{s,t}$	Binary variable that is 1 if charging state of ES s is active, and 0 otherwise	[–]
$v_{c(\theta),t}^{SU/SD}$	Binary variable that is 1 if turbine of TPP c (CSP θ) starts up/shuts down at period t, and 0 otherwise	[–]
$\chi_{d,t}$	Binary variable that is 1 if FD d consumption worst case occurs during period t, and 0 otherwise	[–]
$\chi_{r(\theta),t}$	Binary variable that is 1 if RES r electrical (SF of CSP θ thermal) power production worst case occurs during period t, and 0 otherwise	[–]

Vectors

$\boldsymbol{r}_{c,t} = \{r_{c,t}^{\uparrow}, -r_{c,t}^{\downarrow}, 0\}$	Vector for possible reserve activation scenarios of TPP c	[MW]
$\boldsymbol{r}_{d,t} = \{r_{d,t}^{\uparrow}, -r_{d,t}^{\downarrow}, 0\}$	Vector for possible reserve activation scenarios of FD d	[MW]
$\boldsymbol{r}_{r,t} = \{r_{r,t}^{\uparrow}, -r_{r,t}^{\downarrow}, 0\}$	Vector for possible reserve activation scenarios of RES r	[MW]
$\boldsymbol{r}_{s,t} = \{r_{s,t}^{\uparrow}, -r_{s,t}^{\downarrow}, 0\}$	Vector for possible reserve activation scenarios of ES s	[MW]
$\boldsymbol{r}_t^{SR} = \{r_t^{SR,\uparrow}, -r_t^{SR,\downarrow}, 0\}$	Vector for possible reserve activation scenarios of VPP	[MW]
$\boldsymbol{r}_{\theta,t} = \{r_{\theta,t}^{\uparrow}, -r_{\theta,t}^{\downarrow}, 0\}$	Vector for possible reserve activation scenarios of CSP θ	[MW]

Appendix B. Turn on/off constraints of TPP and CSP

The minimum up and down time requirements for turbines in TPP and CSP (where the index $u \in \mathcal{U}$ covers both $c \in \mathcal{C}$ and $\theta \in \Theta$) are modeled in (B.1a)–(B.1i), following the approach outlined in [35]. Constraints (B.1a) and (B.1b) establish the commitment status of the turbine. Eq. (B.1c) specifies the initial status of the turbine based on N_u^{ON}, which represents the number of initial periods during which the turbine must remain online. Constraint (B.1d) enforces the minimum up time requirement across all subsequent periods defined by UT_u, while constraint (B.1e) applies this requirement to the last $UT_u - 1$ periods. Constraints (B.1f)–(B.1h) are counterparts to (B.1b)–(B.1d), but address the minimum down time requirements. The binary nature of the variables is specified in (B.1i).

$$u_{u,t} - u_{u,t-1} = v_{u,t}^{SU} - v_{u,t}^{SD} \; ; \qquad \forall u,t \qquad \text{(B.1a)}$$

$$v_{u,t}^{SU} + v_{u,t}^{SD} \le 1 \; ; \qquad \forall u,t \qquad \text{(B.1b)}$$

$$\sum_{t=1}^{N_u^{ON}} \left[1 - u_{u,t}\right] = 0 \; ; \qquad \forall u \qquad \text{(B.1c)}$$

$$UT_u \left(u_{u,t} - u_{u,t-1}\right) \le \sum_{t'=t}^{t+UT_u-1} u_{u,t'} \; ; \qquad \forall u, t = N_u^{ON}+1,\dots,T-UT_u+1 \qquad \text{(B.1d)}$$

$$0 \le \sum_{t'=t}^{T} \left[u_{u,t'} - \left(u_{u,t} - u_{u,t-1}\right)\right] \; ; \qquad \forall u, t = T-UT_u+2,\dots,T \qquad \text{(B.1e)}$$

$$\sum_{t=1}^{N_u^{OFF}} u_{u,t} = 0 \; ; \qquad \forall u \qquad \text{(B.1f)}$$

$$DT_u \left(u_{u,t-1} - u_{u,t}\right) \le \sum_{t'=t}^{t+DT_u-1} \left[1 - u_{u,t'}\right] \; ; \qquad \forall u, t = N_u^{OFF}+1,\dots,T-DT_u+1 \qquad \text{(B.1g)}$$

$$0 \le \sum_{t'=t}^{T} \left[1 - u_{u,t'} - \left(u_{u,t-1} - u_{u,t}\right)\right] \; ; \qquad \forall u, t = T-DT_u+2,\dots,T \qquad \text{(B.1h)}$$

$$u_{u,t}, v_{u,t}^{SU}, v_{u,t}^{SD} \in \{0,1\} \; ; \qquad \forall u,t \qquad \text{(B.1i)}$$

Appendix C. Reserve provision capability constraints of units

Constraints (C.1a)–(C.1b) regulate the upward and downward reserves of unit $u \in \mathcal{U}$ – which includes $c \in \mathcal{C}$ for TPP, $\theta \in \Theta$ for CSP, $r \in \mathcal{R}$ for RES, $s \in \mathcal{S}$ for ES, and $d \in \mathcal{D}$ for FD – based on the activation time of the secondary reserve and the ramp rate capabilities of units.

$$r_{u,t}^{\uparrow} \le T^{SR} \bar{R}_u^{SR} \; ; \qquad \forall u,t \qquad \text{(C.1a)}$$

$$r_{u,t}^{\downarrow} \le T^{SR} \underline{R}_u^{SR} \; ; \qquad \forall u,t \qquad \text{(C.1b)}$$

Appendix D. Uncertainties in CSPs thermal production and FDs consumption

The equivalent linear formulation for selecting the worst-case periods in constraint (10e), which address uncertainties in CSPs thermal production, is presented in (D.1).

$$\max \sum_{t' \in \mathcal{T}_\theta, t'=t} \check{P}_{\theta,t'}^{SF} w_{\theta,t'} \; ; \qquad \forall \theta, t \qquad \text{(D.1a)}$$

st.

$$\sum_{t' \in \mathcal{T}_\theta, t'=t} w_{\theta,t'} + \sum_{t' \in \mathcal{T}_\theta, t' \ne t} w_{\theta,t'}^{*} \le \Gamma_\theta \; : \delta_\theta \; ; \qquad \text{(D.1b)}$$

$$0 \le w_{\theta,t'} \le 1 \; : \psi_{\theta,t'} \; ; \qquad \forall t' \in \mathcal{T}_\theta, t' = t \qquad \text{(D.1c)}$$

Similarly, the equivalent linear formulation for selecting the worst-case periods in constraint (10f), which address uncertainties in FDs consumption, is provided in (D.2).

$$\max \sum_{t' \in \mathcal{T}_d, t'=t} \hat{P}_{d,t'} w_{d,t'} \; ; \qquad \forall d,t \qquad \text{(D.2a)}$$

st.

$$\sum_{t' \in \mathcal{T}_d, t'=t} w_{d,t'} + \sum_{t' \in \mathcal{T}_d, t' \ne t} w_{d,t'}^{*} \le \Gamma_d \; : \delta_d \; ; \qquad \text{(D.2b)}$$

$$0 \le w_{d,t'} \le 1 \; : \psi_{d,t'} \; ; \qquad \forall t' \in \mathcal{T}_d, t' = t \qquad \text{(D.2c)}$$

Data availability

Data will be made available on request.

References

[1] Rouzbahani HM, Karimipour H, Lei L. A review on virtual power plant for energy management. Sustain Energy Technol Assessments 2021;47:101370.

[2] European Commission. EU emissions trading system (EU ETS). 2025, URL https://climate.ec.europa.eu/eu-action/eu-emissions-trading-system-eu-ets_en.

[3] Liu X. Research on bidding strategy of virtual power plant considering carbon-electricity integrated market mechanism. Int J Electr Power Energy Syst 2022;137:107891.

[4] Lam LH, Ilea V, Bovo C. European day-ahead electricity market coupling: Discussion, modeling, and case study. Electr Power Syst Res 2018;155:80–92.

[5] ENTSO-E. Entso-e balancing report 2024, european network of transmission system operators for electricity. 2024, URL https://www.entsoe.eu.

[6] European Commission. Report on the functioning of the european carbon market in 2024. 2024, https://climate.ec.europa.eu/eu-action/eu-emissions-trading-system-eu-ets/market-analysis-and-reports_en.

[7] Yu S, Fang F, Liu Y, Liu J. Uncertainties of virtual power plant: Problems and countermeasures. Appl Energy 2019;239:454–70.

[8] Nemati H, Sánchez-Martín P, Sigrist L, Rouco L, Ortega Á. Flexible robust optimization for renewable-only VPP bidding on electricity markets with economic risk analysis. Int J Electr Power Energy Syst 2025;167:110594.

[9] Xiao D, Lin Z, Chen H, Hua W, Yan J. Windfall profit-aware stochastic scheduling strategy for industrial virtual power plant with integrated risk-seeking/averse preferences. Appl Energy 2024;357:122460.

[10] Rahimi M, Ardakani FJ, Ardakani AJ. Optimal stochastic scheduling of electrical and thermal renewable and non-renewable resources in virtual power plant. Int J Electr Power Energy Syst 2021;127:106658.

[11] Foroughi M, Pasban A, Moeini-Aghtaie M, Fayaz-Heidari A. A bi-level model for optimal bidding of a multi-carrier technical virtual power plant in energy markets. Int J Electr Power Energy Syst 2021;125:106397.

[12] Kalantari NT, Abdolahi A, Mousavi SH, Khavar SC, Gazijahani FS. Strategic decision making of energy storage owned virtual power plant in day-ahead and intra-day markets. J Energy Storage 2023;73:108839.

[13] Li Y, Deng Y, Wang Y, Jiang L, Shahidehpour M. Robust bidding strategy for multi-energy virtual power plant in peak-regulation ancillary service market considering uncertainties. Int J Electr Power Energy Syst 2023;151:109101.

[14] Gough M, Santos SF, Javadi MS, Home-Ortiz JM, Castro R, Catalão JP. Bi-level stochastic energy trading model for technical virtual power plants considering various renewable energy sources, energy storage systems and electric vehicles. J Energy Storage 2023;68:107742.

[15] Nemati H, Sánchez-Martín P, Baringo A, Ortega Á. Single-level flexible robust optimal bidding of renewable-only virtual power plant in energy and secondary reserve markets. Energy 2025;328:136421.

[16] Kong X, Xiao J, Liu D, Wu J, Wang C, Shen Y. Robust stochastic optimal dispatching method of multi-energy virtual power plant considering multiple uncertainties. Appl Energy 2020;279:115707.

[17] Zhang J, Liu Z. Low carbon economic dispatching model for a virtual power plant connected to carbon capture system considering green certificates-carbon trading mechanism. Sustain Energy Technol Assessments 2023;60:103575.

[18] Yang D, He S, Chen Q, Li D, Pandžić H. Bidding strategy of a virtual power plant considering carbon-electricity trading. CSEE J Power Energy Syst 2019;5(3):306–14.

[19] Yan Q, Ai X, Li J. Low-carbon economic dispatch based on a CCPP-P2G virtual power plant considering carbon trading and green certificates. Sustainability 2021;13(22):12423.

[20] Liu R, Chen K, Sun G, Lin S, Jiang C. Bidding strategy for the virtual power plant based on cooperative game participating in the electricity-carbon joint market. Int J Electr Power Energy Syst 2024;163:110325.

[21] Zhang L, Liu D, Cai G, Lyu L, Koh LH, Wang T. An optimal dispatch model for virtual power plant that incorporates carbon trading and green certificate trading. Int J Electr Power Energy Syst 2023;144:108558.

[22] Wu Q, Li C, Bai J. Optimal bidding strategy for multi-energy virtual power plant participating in coupled energy, frequency regulation and carbon trading markets. Int J Hydrog Energy 2024;73:430–42.

[23] Ghasemi Olanlari F, Amraee T, Moradi-Sepahvand M, Ahmadian A. Coordinated multi-objective scheduling of a multi-energy virtual power plant considering storages and demand response. IET Gener Transm Distrib 2022;16(17):3539–62.

[24] Ju L, Yin Z, Zhou Q, Li Q, Wang P, Tian W, Li P, Tan Z. Nearly-zero carbon optimal operation model and benefit allocation strategy for a novel virtual power plant using carbon capture, power-to-gas, and waste incineration power in rural areas. Appl Energy 2022;310:118618.
[25] Ju L, Lv S, Zhang Z, Li G, Gan W, Fang J. Data-driven two-stage robust optimization dispatching model and benefit allocation strategy for a novel virtual power plant considering carbon-green certificate equivalence conversion mechanism. Appl Energy 2024;362:122974.
[26] Alabi TM, Lu L, Yang Z. Data-driven optimal scheduling of multi-energy system virtual power plant (MEVPP) incorporating carbon capture system (CCS), electric vehicle flexibility, and clean energy marketer (CEM) strategy. Appl Energy 2022;314:118997.
[27] Chang W, Yang Q. Low carbon oriented collaborative energy management framework for multi-microgrid aggregated virtual power plant considering electricity trading. Appl Energy 2023;351:121906.
[28] Yan Q, Zhang M, Lin H, Li W. Two-stage adjustable robust optimal dispatching model for multi-energy virtual power plant considering multiple uncertainties and carbon trading. J Clean Prod 2022;336:130400.
[29] Tan C, Wang J, Geng S, Pu L, Tan Z. Three-level market optimization model of virtual power plant with carbon capture equipment considering copula–cvar theory. Energy 2021;237:121620.
[30] Chen Y, Niu Y, Qu C, Du M, Liu P. A pricing strategy based on bi-level stochastic optimization for virtual power plant trading in multi-market: Energy, ancillary services and carbon trading market. Electr Power Syst Res 2024;231:110371.
[31] Wei X, Xu Y, Sun H, Bai X, Chang X, Xue Y. Day-ahead optimal dispatch of a virtual power plant in the joint energy-reserve-carbon market. Appl Energy 2024;356:122459.
[32] Naval N, Yusta JM. Virtual power plant models and electricity markets-a review. Renew Sustain Energy Rev 2021;149:111393.
[33] Nemati H, Sánchez-Martín P, Ortega Á, Sigrist L, Lobato E, Rouco L. Flexible robust optimal bidding of renewable virtual power plants in sequential markets under asymmetric uncertainties. Sustain Energy, Grids Networks 2025;101801.
[34] European Environment Agency. Emissions trading viewer - dashboards. 2024, URL https://www.eea.europa.eu/en/analysis/maps-and-charts/emissions-trading-viewer-1-dashboards.
[35] Carrión M, Arroyo JM. A computationally efficient mixed-integer linear formulation for the thermal unit commitment problem. IEEE Trans Power Syst 2006;21(3):1371–8.
[36] Nemati H, Sigrist L, Rodríguez LR, Sánchez-Martín P, Ortega Á. Addressing unfeasibilities of energy storage systems participating in energy and reserve markets. In: 2022 IEEE PES innovative smart grid technologies conference europe (ISGT-europe). IEEE; 2022, p. 1–5.
[37] García IL, Álvarez JL, Blanco D. Performance model for parabolic trough solar thermal power plants with thermal storage: Comparison to operating plant data. Sol Energy 2011;85(10):2443–60.
[38] Ortega Á, Oladimeji O, Nemati H, Sigrist L, Sánchez-Martín P, Rouco L, et al. Modeling of VPPs for their optimal operation and configuration. Tech. rep. POSYTYF Consortium, deliverable 5.1., 2021.
[39] Zhang Z, Zhou M, Wu Z, Liu S, Guo Z, Li G. A frequency security constrained scheduling approach considering wind farm providing frequency support and reserve. IEEE Trans Sustain Energy 2022;13(2):1086–100.
[40] Yin S, Wang J, Li Z, Fang X. State-of-the-art short-term electricity market operation with solar generation: A review. Renew Sustain Energy Rev 2021;138:110647.
[41] Bertsimas D, Sim M. The price of robustness. Oper Res 2004;52(1):35–53.
[42] Floudas CA. Nonlinear and mixed-integer optimization: fundamentals and applications. Oxford University Press; 1995.
[43] Wen Y, AlHakeem D, Mandal P, Chakraborty S, Wu Y-K, Senjyu T, Paudyal S, Tseng T-L. Performance evaluation of probabilistic methods based on bootstrap and quantile regression to quantify PV power point forecast uncertainty. IEEE Trans Neural Networks Learn Syst 2019;31(4):1134–44.
[44] Ciemat Spain. PV-STU production forecast. URL https://www.ciemat.es/.
[45] Iberdrola Spain. Wind production forecast. URL https://www.iberdrola.es/.
[46] International Energy Agency. Levelised cost of electricity calculator. 2023, URL https://www.iea.org/data-and-statistics/data-tools/levelised-cost-of-electricity-calculator.
[47] Red Eléctrica de España (REE). Electricity Market Data. URL https://www.esios.ree.es/.
[48] International Carbon Action Partnership. ETS prices. 2023, URL https://icapcarbonaction.com/en/ets-prices.